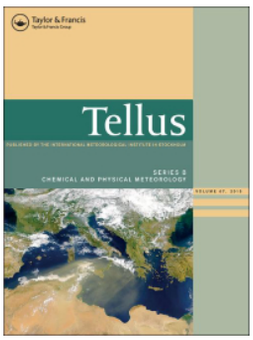

Tellus B: Chemical and Physical Meteorology

ISSN: (Print) (Online) Journal homepage: https://www.tandfonline.com/loi/zelb20

Role of river discharge and warming on ocean acidification and pCO_2 levels in the Bay of Bengal

B. Sridevi & V. V. S. S. Sarma

To cite this article: B. Sridevi & V. V. S. S. Sarma (2021) Role of river discharge and warming on ocean acidification and pCO_2 levels in the Bay of Bengal, Tellus B: Chemical and Physical Meteorology, 73:1, 1-20, DOI: 10.1080/16000889.2021.1971924

To link to this article: https://doi.org/10.1080/16000889.2021.1971924

Published online: 01 Sep 2021.

Tellus SERIES B CHEMICAL AND PHYSICAL METEOROLOGY
PUBLISHED BY THE INTERNATIONAL METEOROLOGICAL INSTITUTE IN STOCKHOLM

Role of river discharge and warming on ocean acidification and pCO_2 levels in the Bay of Bengal

By B. SRIDEVI[1], and V. V. S. S. SARMA[1,2]*, [1]*CSIR-National Institute of Oceanography, Visakhapatnam, India;* [2]*Academy of Scientific and Innovative Research (AcSIR), Dona Paula, Goa, India*

(Manuscript received 8 June 2020; in final form 19 August 2021)

ABSTRACT

Shifts in surface ocean pCO_2 and pH are important controls governing global climate. Based on the linear relationship of observed surface pH and pCO_2 with sea surface temperature (SST), sea surface salinity (SSS) and Chlorophyll-a (Chl-a) multiple linear regression equations were developed. Based on remote sensing SST, Chl-a and model-derived SSS, pH and pCO_2 data were derived from 1998 to 2015. Overall warming of BoB is noticed at the rate of 0.004° to 0.03 °C/y whereas cooling is found in the northwestern BoB during winter and spring seasons associated with an increase in atmospheric dust. Decrease in SSS is noticed during all seasons due to melting of Himalayan ice cover associated with increase in fresh water flux due to increase in atmospheric temperature. Increase in pH is observed in the eastern and southern Bay during all seasons associating with warming and decrease in salinity. In contrast, decrease in pH ($-0.001\,y^{-1}$) and pCO_2 increase ($+0.1$ to $+0.7$ µatm y^{-1}) is noticed in the western and head Bay during winter and spring seasons due to deposition of atmospheric pollutants. This study suggests that increase in freshwater input due to melting of Himalayan ice cover and deposition of atmospheric pollutants are dominant controlling factors on surface ocean pH and pCO_2 in the BoB between 1998 and 2015 and this region is acting as a stronger sink for the atmospheric CO_2 in the present than that in the past two decades. The global coastal regions are significantly influenced by river discharge and atmospheric deposition of pollutants and they are not part of the global models leading to ill-reproduction of seasonal variability in pH and pCO_2. Inclusion of these processes may improve prediction of pH and pCO_2 in the regions heavily influenced by discharge/deposition from land and atmosphere.

Keywords: ocean acidification, pH, pCO_2, atmospheric dust, climate change

1. Introduction

Atmospheric carbon dioxide (CO_2) is being increased at the rate of >2 ppm/y (Dlugokencky and Tans, 2020). Increase in CO_2 by ~48% is reported from pre-industrial era (277 ppm in 1750; Joos and Spahni, 2008) to recent (411 ppm in 2020; Dlugokencky and Tans, 2020) due to combustion of fossil fuels and land use changes. The rate of decrease has been estimated at between −0.0026 and $-0.0003\,y^{-1}$ (Bates et al., 2014; Lauvset et al., 2015). Higher rate of acidification is reported in the coastal region due to multiple human activities that modify carbonate equilibrium (e.g. Doney, 2010; Cai et al., 2011, 2020; Hall et al., 2020). While absorption of anthropogenic CO_2 dominates Ocean Acidification (OA) on global scale, the other anthropogenic sources such as deposition of atmospheric pollutants, viz., sulphate and nitrate aerosols formed through fossil fuel and biomass burning, also play a key role on OA in the highly urbanized or populated regions (Mackenzie et al., 1995; Schlesinger, 1997; Doney et al., 2007). Rapid increase in atmospheric pollution is reported over the globe with higher increase over Bay of Bengal (BoB) (Zhang and Reid, 2010). Since the lifetime of atmospheric pollutants is quite short (a few days to a week), they will be deposited close to their source(s), primarily the surrounding land and coastal ocean (NAPAP, 1991; Howarth et al., 1996; Rodhe et al., 2002; Dentener et al., 2006), resulting possible decrease in coastal pH. Based on numerical

*Corresponding author. email: sarmav@nio.org

Citation: Tellus B: 2021, **73**, 1971924, https://doi.org/10.1080/16000889.2021.1971924

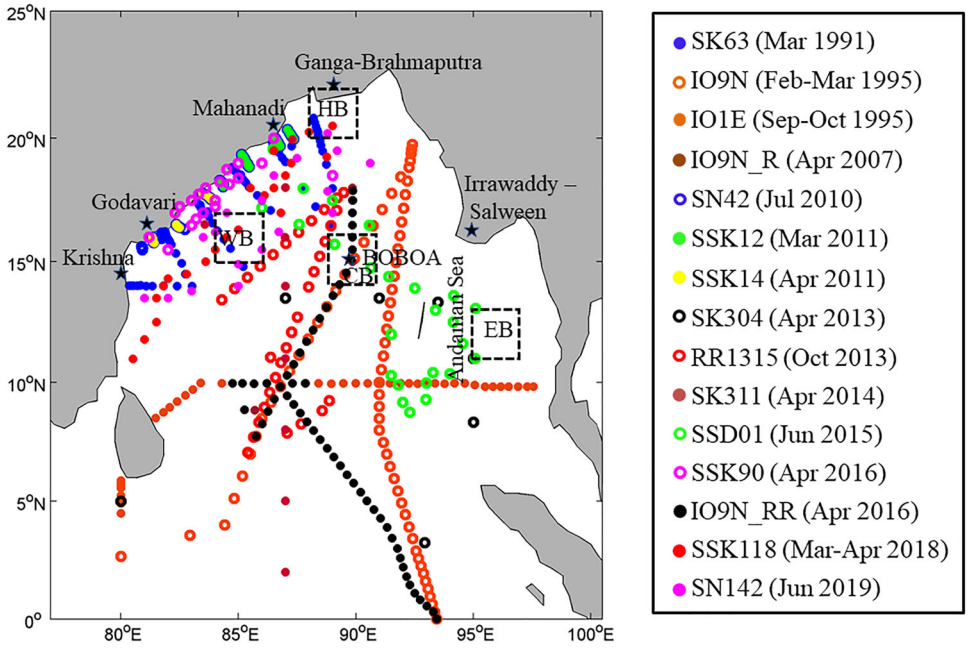

Fig. 1. The map showing the station locations of the data used for construction of multiple regression equations for the Bay of Bengal. The data collected during different periods and years are given in different colors indicated in the box. The locations of discharge by different rivers are shown. The boxes 1, 2, 3, 4 and 5 represent head bay (HB), western bay (WB), central bay (CB), and eastern bay (EB), respectively.

models, Doney et al. (2007) suggested that atmospheric inputs of nitric acid (HNO3), sulfuric acid (H2SO4) and ammonia (NH3) substantially alter pH in the coastal waters, in addition to large-scale climate changes. They further noticed that decrease in pH by up to −0.003 is estimated due to atmospheric deposition of nitrogen and sulfur between 1990 and 2000. In addition, sewage and agricultural discharges bring nutrients, whereas allochthonous and soil organic matter through river runoff that stimulates autochthonous production/decomposition in the coastal waters that modify pH in the coastal waters (Howarth et al., 2002; Cai et al., 2020).

The Bay of Bengal (BoB) is the region surrounded by land-masses of India and south-east Asia on three directions and receives large amount of terrigenous material, including pollutants via rivers. It also experiences atmospheric pollution as a result of about one third of the world's population is living along its coast. The second largest riverine system in the world, the Ganges-Brahmaputra system, discharge huge amount of freshwater to the BoB and brings in significant amount of organic and nutrient pollutants (Krishna et al., 2015, 2016; Sarma et al., 2020). Mukhopadhyay et al. (2002) noticed that pH in the Hooghly (Ganges) estuary is high (8.13–8.15) with undersaturated pCO_2 levels during monsoon and contrasting to that noticed during non-monsoon period. Samanta et al. (2015) noticed the lowest concentration of dissolved inorganic carbon (DIC) during monsoon and the highest during non-monsoon period in the Hooghly (Ganges) estuary. Since discharge peaks during monsoon, pCO_2 levels decrease in the BoB resulting in linear relationship between salinity and pCO_2 levels (Kumar et al., 1996; Sarma et al., 2012a). Based on monthly time-series observations, Sarma et al. (2018) reported positive correlation between the observed salinity and pCO_2 and inverse relation with pH in the coastal BoB. They further noticed that the variability in pCO_2 along the coastal BoB is governed by direction of East India Coastal Currents (EICC) that brings in low salinity waters influenced by Ganges discharge during October - January period resulting in high pH, and low pCO_2, and contrasting to that noticed during February-May due to change in direction of EICC. Therefore, the magnitude of freshwater discharge may change pH and pCO_2 of surface waters in the BoB.

Aerosol Optical Depth (AOD) is the measure of aerosols (e.g. urban haze, smoke particles, desert dust, sea salt) distributed within a column of air. The highest AOD is observed over the Indian subcontinent and BoB followed by South China Sea. The rate of increase in AOD between 2000 and 2009 is the highest over BoB than elsewhere in the world (Zhang and Reid, 2010). Kumar et al. (2008) estimated high non-sea salt sulphate in the marine atmospheric boundary layer over the BoB indicating that

Table 1. Cruise name, region, period and reference where data were published of the data collected in the Bay of Bengal.

Cruise name	Area of sampling	Year and month of sampling	Publication reference
SK63	Western BoB	March 1991	Kumar et al. (1996)
I09N	Central and eastern BoB	February–March 1995	Sabine et al. (2000)
I01E	Southern BoB	September–October, 1995	Sabine et al. (1999, 2000)
I09N_R	Central and eastern BoB	April, 2007	Unpublished
SN42	Western BoB	July 2010	Sarma et al. (2012a)
SSK12	Western coastal BoB	March 2011	Unpublished
SSK14	Western coastal BoB	April 2011	Unpublished
SK304	Central BoB and Andaman Sea	April 2013	Unpublished
RR1315	Central BoB	October 2013	Unpublished
SK311	Central BoB	April 2014	Unpublished
SSD01	Central BoB and Andaman Sea	June 2015	Unpublished
SSK90	Western BoB	April 2016	Unpublished
I09N_RR	Central and eastern BoB	April 2016	Unpublished
SSK118	Western and Central BoB	Mar–April 2018	Sarma et al. (2019)
SN142	Western and Central BoB	June 2019	Unpublished
BOBOA	Central Bay of Bengal	Nov 2013–present	Unpublished

this region receives more pollutants during January - April period when air flows dominantly from land to sea (continental flow). Based on data collected during 1991 and 2011; Sarma et al. (2015) found that rapid decrease in pH ($0.007\,y^{-1}$) occurred in the northwestern coastal BoB during spring (March-April) and attributed to the deposition of atmospheric pollutants. They further noticed that northwestern BoB acted as a sink for atmospheric CO_2 during spring intermonsoon of 1991, but it was turned to source during 2011 (Kumar et al., 1996; Sarma et al., 2015). However, the changes in pH in the other parts of the BoB, seasons and exact rate of changes are unknown due to lack of time-series data.

Dinesh Kumar et al. (2016) found that BoB is warming at the rate of 0.07 °C/decade based on long-term SST data between 1940 and 2009. Using reanalysis salinity data, Dinesh Kumar et al. (2016) reported an increasing trend in SSS in the BoB between 1940 and 1972 and a decreasing trend from 1973 to 2008. Based on IPCC (2013) reports, the average surface atmospheric temperature is increased by 0.85 °C since 1860 over India and the Global temperatures increased by 0.6 ± 0.2 °C since 1990 (Lozan et al., 2001). This may be the prime reason for the increase of retreating of Himalayan glaciers, which contribute to a decrease in salinity in the BoB (Roxy et al., 2015b; Paul, 2018). This is further confirmed by Goes et al. (2020), who found that decrease in snow cover over the Himalayas due to climate change and it is consistent with the Trott et al. (2019), who reported an increasing trend in the freshwater flux into the BoB over the period of 1955–1995. Dandapat et al. (2020) found that modification of salinity has significant impact on stratification and heat flux in the BoB. As noticed by Sarma et al. (2018), the decrease in salinity increases pH and decreases pCO_2 levels, therefore, increase in river discharge may decrease OA and pCO_2 levels. The main objective of this work is to evaluate impact of warming, melt-driven freshening and atmospheric dust deposition on pCO_2 and OA in the BoB.

2. Material and methods

2.1. Data collection and methodology

The BoB was sampled during different seasons (winter, spring, summer and fall monsoons) for temperature, salinity, nutrients (phosphate and silicate), pH, and dissolved inorganic carbon (DIC) in the BoB between 1991 and 2019 by our group (Fig. 1; Table 1). In addition to this, we have also used World Ocean Circulation Experiment (WOCE) data available at www.nodc.noaa.gov/woce (Fig. 1; Table 1) for this study. Samples were collected in the entire water column during different expeditions but we have used only mixed layer data for this study. Temperature and salinity data obtained using conductivity, temperature and pressure (CTD) sensors (Sea Bird Electronics) with the detection limits of ±0.0005 S/m, ±0.001 °C and ±0.1 m respectively. Nutrients, phosphate and silicate, were analyzed following colorimetric technique of Grasshoff et al. (1983) with the detection limits of ±0.018 and ±0.02 µM respectively. Chlorophyll-a (Chl-a) was estimated using spectrofluorometric technique following extraction of Chl-a in to N,N-dimethylformamide (Suzuki and Ishimatu, 1990). pH data was collected using multiwavelength spectrophotometric method involving in cresol purple whereas dissolved inorganic carbon was measured following Coulometer (Sarma et al., 1998). The pCO_2 data was computed based on measured DIC, pH

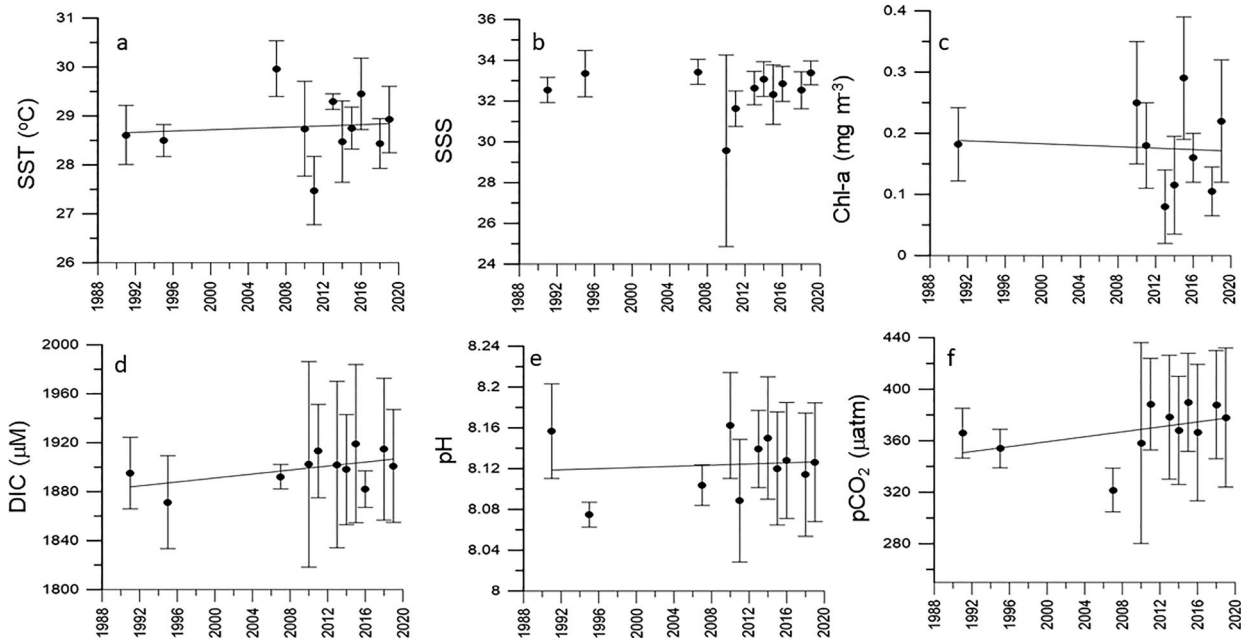

Fig. 2. Mean (standard deviation) of measured (a) SST, (b) SSS, (c) Chl-a, (d) DIC, (e) pH and (f) pCO_2 are depicted with reference to year of collection in the Bay of Bengal.

and dissociation constants given by Millero et al. (2006) using CO_2 sys program (Lewis and Wallace, 1998). The estimated error on pH, and DIC was 0.005 and 2 µM respectively using Certified Reference Material (CRM) supplied by Dr. A.G. Dickson, Scripps Institute of Oceanography, USA, whereas 9 µatm on estimated pCO_2. Certified Reference Materials (CRMs) were used in all cruises except during 1991 cruise due to unavailability and this data were corrected using deep water samples comparing with World Ocean Circulation Experiment (WOCE- transect I09N_1995) samples based on cross-over stations in the central BoB. The difference between these two observations in DIC was within ±4 µmol/kg.

2.2. Model description

2.2.1. Observed trends of DIC, pH, and pCO_2 in the BoB. The details of the period and region of data collection of DIC and pH were given in Table 1 along with published information. The mean measured data of SST, SSS, DIC, pH and computed pCO_2 during different years in the BoB is plotted in Fig. 2 to examine the long-term variability. Based on this data, SST increased at the rate of $+0.0065\,^{\circ}C\ yr^{-1}$ whereas SSS and Chl-a decreased at the rate of $-0.0063\,y^{-1}$ and $-0.0006\,mg\ m^{-3}\ y^{-1}$ respectively. In case of DIC, pH and pCO_2, the rate of increase was $+0.81\,\mu mol\ kg^{-1}\ y^{-1}$, $+0.0003\,y^{-1}$ and $0.76\,\mu atm\ y^{-1}$ respectively. None of these rates are statistically significant as the data are highly biased with reference to season and region (see Table 1), hence deriving the long-term trends using such data may not yield appropriate rates. Hence, high-resolution temporal and spatial data are needed to generate long-term changes in inorganic carbon system.

2.2.2. Multiple linear regression (MLR) approach. Multiple regression equations were developed based on the long-term data of surface water temperature, salinity, pH and pCO_2 in the BoB during different seasons between 1991 and 2019 (Fig. 1). pH and pCO_2 in the BoB showed significant spatial variability due to river discharge from major rivers such as Ganges, Brahmaputra and Irrawady-Salween riverine systems. The data collected in the central or southern BoB, which is away from the river discharge region, yields different relationship due to weak influences of river discharge. For instance, Surface Ocean Carbon Atlas (SOCAT) data mainly comes from the international waters (outside Exclusive Economic Zone (EEZ); Bakker et al., 2016, 2020) where salinity varied between 32 and 34. In such region, linear relationship between SST and pCO_2 is found (figure is not shown). In contrast, salinity in the BoB goes down to 20 in the northern and coastal BoB, where influence of discharge is more and contributes to >50% surface area. The controlling mechanisms of SST are different in the freshwater influenced than weakly stratified regions in the BoB. For instance, in the highly stratified regions due to freshwater, the changes in SST

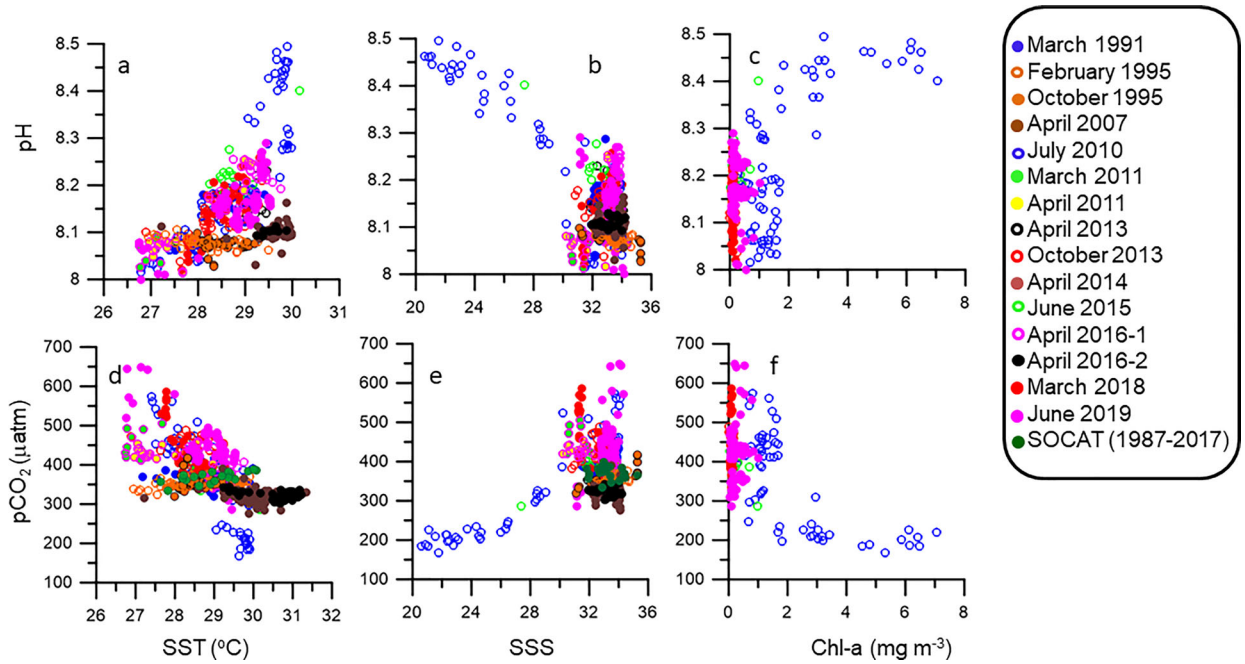

Fig. 3. The relationship of pH with (a) SST, (b) SSS and (c) Chl-a and relationship of pCO_2 with (d) SST, (e) SSS and (f) Chl-a in the Bay of Bengal. The color code of the figure is given in the box.

reflect strength of the stratification and therefore magnitude of discharge/salinity whereas vertical mixing is represented in the weakly stratified regions. Since freshwater bring low pCO_2 and DIC waters associated with warming due to stratification, SST and pCO_2 displays inverse relationship. Similarly, SSS displayed linear relationship with DIC (Fig. S1, supplementary material). Therefore, the selection data is very important on identifying the relationship between physical and inorganic carbon components in the BoB. Therefore, we included data collected from various regions and seasons covering entire BoB including the regions influenced by various magnitude of discharge by different rivers to constructs MLR equations.

Surface water pH and pCO_2 showed distinct relationships with SST, SSS and chlorophyll-a. pH displayed linear relationship with SST ($r^2 = 0.78$; $p < 0.001$; Fig. 3a) and strong inverse relationship with SSS ($r^2 = 0.86$; $p < 0.001$; Fig. 3b) as freshwater from Ganges river is relatively high compared to seawater (Sarma et al., 2012a, 2018). Since warming of surface ocean in the northern BoB occurs due to salinity stratification, higher warming associated with low saline water. Chl-a displayed linear relationship with pH ($r^2 = 0.42$; $p < 0.01$) as increase in primary production increases pH (Fig. 3c). In contrast, pCO_2 shows inverse relationship with SST ($r^2 = 0.77$; $p < 0.001$; Fig. 3d) and linear positive relationship with salinity ($r^2 = 0.81$; $p < 0.001$; Fig. 3e) as low saline waters contain low pCO_2, and due to mixing/stratification of water column modified pCO_2 levels. Chl-a displayed inverse relationship with pCO_2 ($r^2 = 0.38$; $p < 0.01$; Fig. 3f) due to increase in primary production decreases pCO_2. The t-test revealed that slope and intercepts of these relations, however, did not show significant seasonal variations. The resultant regression fits with annual data are:

$$\mathrm{pH} = 7.59 + 0.043 * \mathrm{SST} - 0.023 * \mathrm{SSS} + 0.0024 * \mathrm{Chl} \left(r^2 = 0.78; p < 0.001\right) \quad (1)$$

$$\mathrm{pCO_2} = 816.62 - 43.27 * \mathrm{SST} + 24.77 * \mathrm{SSS} + 9.37 * \mathrm{Chl} \left(r^2 = 0.81; p < 0.001\right) \quad (2)$$

The seasonal variability in temperature ranges between 23 °C and 30 °C whereas salinity ranges between 26 and 34 psu. The variability in SST more influence on pH and pCO_2 than salinity, and the impact of Chl-a is much smaller in the BoB.

2.3. Remote sensing/model data and methodology

Data from multiple sources are utilized to carry out the present study. The primary data used is daily microwave Optimally Interpolated Sea Surface Temperature (SST) analysis data (AVHRR + AMSR-E products) from the

NOAA Satellite with resolution of 0.25° × 0.25° during the period 1998–2015. This data are collected from APDRC (Asia-Pacific Data-Research Center) (http://apdrc.soest.hawaii.edu/las8). Global Ocean monthly reanalysis Sea Surface Salinity (SSS) is taken from CMEMS (Copernicus Marine Environment Monitoring Service) (http://marine.copernicus.eu/services) with a resolution of 0.25° × 0.25° during the period 1998–2015. This reanalysis is performed with NEMOv3.1 ocean model. This model is forced by ERA-Interim atmospheric variables covering the time period 1993 to 2015 and data is assimilated using Sea-Ice concentration, Sea surface temperature, sea level anomaly and *in-situ* temperature and salinity profiles. The European space agency with Ocean Colour CCI (OC_CCI) project derived the chlorophyll (Chl) data by merging the SeaWiFS, MODIS and MERIS data. This merged monthly chlorophyll data is taken from OCCCI_v3.0 during the period 1998–2015 (ftp://oc-cci-data:ELaiWai8ae@oceancolour.org) with a spatial resolution of 0.08 × 0.08° (9 × 9 km). Monthly Aerosol Optical Depth (AOD) data at 550 nm wave length is taken from MODIS-Terra satellite (https://oceandata.sci.gsfc.nasa.gov) with a resolution of 1° × 1° during the period 2001–2015. All the data have been gridded to uniform grid resolution of 0.25 × 0.25°.

We have used measured pCO_2 data between November 2013 and June 2015 from Bay of Bengal Ocean Acidification buoy (BOBOA) (https://www.ncei.noaa.gov/access/ocean-carbon-data-system/oceans/Moorings/BOBOA.html; Sutton et al., 2017) for calibration of model. The high time-resolution data was averaged to monthly mean and pH and pCO_2 is computed based on monthly mean satellite derived SST, SSS and Chl-a. Climatology of SOCAT data was obtained from Landschutzer et al. (2020) (https://www.nodc.noaa.gov/ocads/oceans/MPI-ULB-SOM_FFN_clim.html) and Takahashi climatology is obtained from Takahashi et al. (2009, 2014) (https://www.ldeo.columbia.edu/res/pi/CO2/carbondioxide/air_sea_flux/month_flux_2006c.txt).

2.4. Deriving long-term trends

Long-term changes in the seasonal observations are analyzed using the linear trend analysis for each parameter at each and every grid point. To facilitate the analysis, we averaged data to represent different seasons such as winter (December, January and February), spring (March, April and May), summer (June, July, August and September) and fall monsoon (October and November) seasons. To understand the relation between SST and AOD, seasonal regression analysis is performed between the SST and AOD during the period between 2001 and 2015.

3. Results

3.1. Long-term variability in SST, SSS, Chl-a and AOD

Long-term (18 years) variability in SST between 1998 and 2015 revealed that the entire BoB is warming, however, the rate of warming displayed large seasonal and spatial variability (Fig. S2, supplementary material). During winter, for instance, the Bay cools at the rate of $-0.02\,^{\circ}C\ y^{-1}$ in the northwestern region whereas it warms in the remaining part of Bay ($+0.03\,^{\circ}Cy^{-1}$). The warming rate is significant at 90% confidence level whereas the cooling rate is significant at 85% (Fig. S1). The region of cooling in the northwestern Bay expanded at the rate $-0.02\,^{\circ}C\ y^{-1}$ whereas significant warming is restricted to the southeastern Bay during spring. The entire Bay is warmed at the rate of $+0.02$ to $+0.04\,^{\circ}C\ y^{-1}$ during summer, including the head Bay region with more significant rate is noticed in the north and southeastern Bay at 90% significance. The rate of warming increases to $+0.05\,^{\circ}C\ y^{-1}$ during fall monsoon in the entire Bay, except at the head Bay, where SST cools at the rate of $-0.03\,^{\circ}C\ y^{-1}$ (Fig. S1).

The long-term changes in SSS indicated decrease in the northern Bay and increase in the southern Bay (Fig. S3, supplementary material), except at the few pockets where the trends are below 90% significant level. During winter monsoon season, the northern Bay and Andaman Sea displayed decrease in salinity (freshening) at the rate of $> -0.03\,y^{-1}$ at 90% significant level, except at head Bay. In contrast, significant salting is observed in the southern Bay (south of 15°N) at the rate of $+0.03\,y^{-1}$. The region of dilution is expanded during spring to almost entire northern BoB and Andaman Sea whereas salting region is restricted to southwestern Bay (Fig. S3). The rate of freshening in the Andaman Sea and salting in the southwestern Bay is significant at 90% levels whereas freshening in the northern Bay is at 85% significance. Significant variability in SSS is not noticed in the equatorial region (0–5°N). The spatial variability in SSS during summer is close to that of winter but the rate of change is much smaller and significant at 80% level only. On the other hand, increasing in SSS is observed in the entire basin, except in the Andaman Sea but significant levels are low (<80%) during fall monsoon.

Irrespective of the season, Chl-a is decreased almost in the entire Bay but with 90% significant level in the eastern and southern Bay during winter, spring and summer monsoons. In contrast, a decreasing trend ($-0.01\ mg\ m^{-3}\ y^{-1}$) was observed during fall monsoon in the southern Bay but the changes are not significant in the northern and central Bay (Fig. S4, supplementary material).

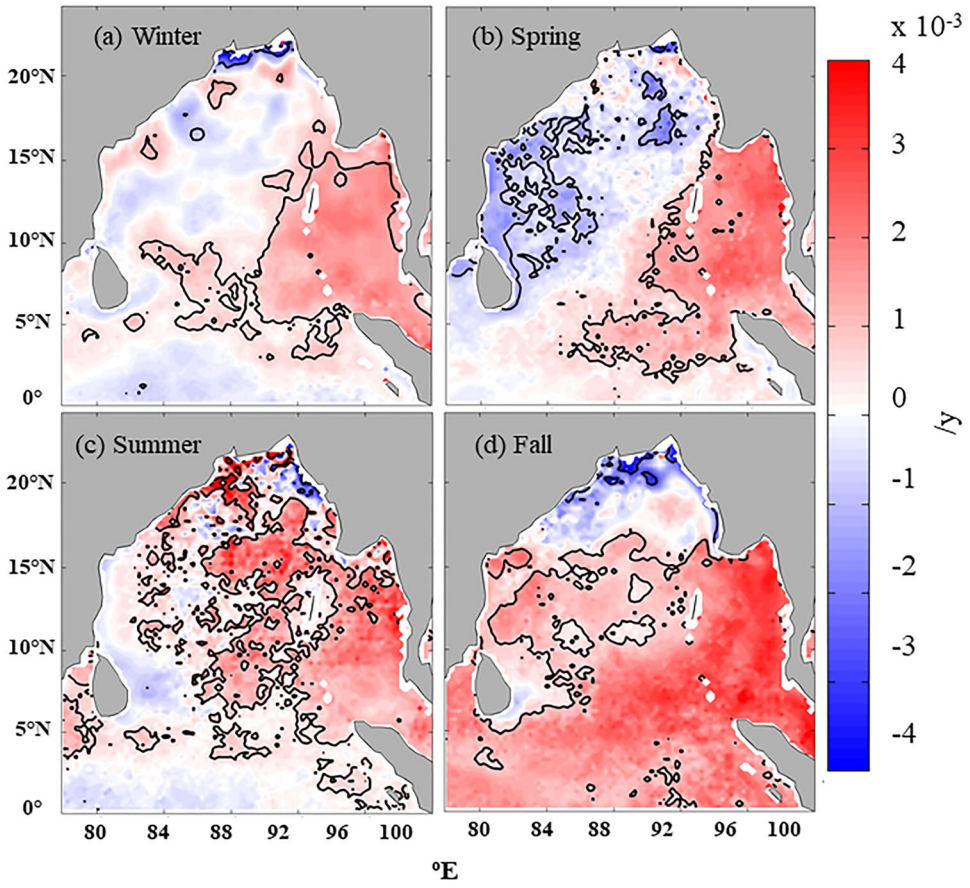

Fig. 4. Seasonal mean rate of increase (positive) or decrease (negative) of pH (in 10^{-3}) during (a) winter, (b) spring, (c) summer and (d) fall monsoons in the Bay of Bengal. The region within the thick contour lines shows 90% significant level.

The AOD showed an increasing trend in the entire BoB with more significant increase (>90% significant levels) in the northern and western Bay during winter and spring seasons (Fig. S5, supplementary material). Significant increase in AOD is noticed in the equatorial belt and western Bay during summer and fall seasons. The AOD variability in the central Bay is not significant.

3.2. Seasonal and long-term variability in pH and pCO_2

A decrease in pH at the rate of $-0.001\,y^{-1}$ is observed in the western Bay between 1998 and 2015 during winter and spring seasons at ~80% significant level (Fig. 4). In contrast, an increasing trend in pH is observed at the rate of $+0.002\,y^{-1}$ to $+0.003\,y^{-1}$ in the eastern Bay during all seasons. Significant decreasing trend in pH (-0.003 to $-0.001\,y^{-1}$) is observed in the head Bay during winter and fall seasons (Fig. 4; Table 2) in association with low salinity (Fig. S3). Overall, increasing trend in pH is dominant in the BoB in association with warming and freshening of waters (Figs. S2 and S3).

The variations in pCO_2 between 1998 and 2015 showed increasing trend at the rate of +0.1 to +0.7 μatm y^{-1} in the western Bay during winter and spring seasons at ~80% significant levels, whereas perennial decreasing trend is noticed in the eastern Bay (−1.9 to −2.9 μatm y^{-1}) with 95% significant level and similar trend is noticed in the central Bay (−0.2 to −1.9 μatm y^{-1}) with less significance (Fig. 5; Table 2). The increasing trend is observed during fall and winter monsoon (+2.4 and +1.3 μatm y^{-1} respectively) and decreasing trend during spring and summer (−0.2 and −1.6 μatm y^{-1} respectively) in the head bay. Annually, a decrease in pCO_2 trend is observed at the rate of −0.7 μatm y^{-1} in the entire BoB (Fig. 5).

Based on the basin-wise trends, the western (WB) is contrasting to that of eastern BoB (EB) and behaves significantly different from that of central Bay (CB) due to variable sources of freshwater due to influence of Irrawady-Salween river system and Indian peninsular rivers respectively in EB and WB regions whereas head Bay (HB) is significantly influenced by discharge from Ganga-Brahmaputra rivers. In order to examine the variability in pH and pCO_2, the seasonal variability and long-term

Table 2. Mean values of SST, SSS, AOD, Chl-a, pH and pCO_2 and rate of change between 1998 and 2015 in the selected regions in the Bay of Bengal (EB: 11–13°N; 95–97°E; WB: 15–17°N; 84–86°E; HB: 20–22°N; 88–90°E; CB: 14–16°N; 89–91°E).

Parameter	Season	Mean				Slope (/year)				*p*-value			
		EB	WB	CB	HB	EB	WB	CB	HB	EB	WB	CB	HB
SST (°C)	DJF	28.12	26.81	27.11	24.97	+0.020	−0.011	+0.012	−0.004	0.24	0.39	0.49	0.69
	MAM	29.62	29.01	29.01	28.24	+0.034	−0.015	+0.002	+0.010	0.11	0.25	0.70	0.55
	JJAS	28.52	28.95	28.74	29.14	+0.029	+0.019	+0.025	+0.058	0.10	0.13	0.07	0.00
	ON	28.66	28.69	28.86	28.57	+0.047	+0.005	+0.021	−0.021	0.01	0.63	0.06	0.25
SSS (psu)	DJF	31.31	32.88	32.39	28.90	−0.041	−0.017	+0.022	+0.053	0.07	0.39	0.20	0.40
	MAM	31.92	33.18	32.43	31.90	−0.027	−0.018	−0.0033	−0.013	0.08	0.20	0.73	0.64
	JJAS	31.49	33.30	32.98	25.61	−0.017	+0.004	+0.0020	−0.004	0.44	0.74	0.74	0.58
	ON	30.50	32.00	32.63	22.38	−0.029	−0.010	−0.0011	+0.081	0.47	0.72	0.85	0.36
Chl (mg/m^3)	DJF	0.20	0.25	0.18	1.55	−0.001	−0.0002	−0.0004	+0.060	0.62	0.41	0.54	0.42
	MAM	0.18	0.16	0.15	1.84	−0.001	−0.001	−0.0008	−0.038	0.42	0.52	0.18	0.46
	JJAS	0.19	0.25	0.16	2.33	−0.001	−0.002	−0.0003	−0.016	0.35	0.46	0.43	0.40
	ON	0.19	0.26	0.16	1.88	+0.001	+0.008	+0.0015	−0.015	0.41	0.15	0.35	0.37
AOD (at 550 nm)	DJF	0.31	0.36	0.27	0.58	+0.001	+0.008	+0.0052	+0.017	0.55	0.00	0.02	0.00
	MAM	0.36	0.47	0.36	0.63	+0.005	+0.009	+0.0066	+0.012	0.07	0.02	0.04	0.00
	JJAS	0.34	0.49	0.41	0.57	−0.001	+0.005	+0.0015	+0.010	0.69	0.28	0.65	0.29
	ON	0.27	0.33	0.25	0.44	+0.001	+0.010	+0.0033	+0.016	0.77	0.00	0.28	0.00
pH	DJF	8.08	7.99	8.01	7.99	+0.0018	−0.001	+0.0001	−0.0011	0.05	0.21	0.70	0.48
	MAM	8.13	8.07	8.09	8.06	+0.0020	−0.001	+0.0002	−0.0002	0.05	0.20	0.74	0.57
	JJAS	8.09	8.07	8.07	8.27	+0.0019	+0.001	+0.0019	+0.0014	0.07	0.19	0.12	0.45
	ON	8.12	8.09	8.08	8.29	+0.0028	+0.001	+0.0009	−0.0025	0.01	0.37	0.20	0.20
pCO_2 (μatm)	DJF	377	473	447	472	−1.9	+0.1	−0.1	+1.3	0.06	0.62	0.68	0.47
	MAM	328	387	368	408	−2.1	+0.7	−0.2	+0.2	0.05	0.33	0.74	0.59
	JJAS	362	391	392	196	−2.0	−0.7	−1.9	−1.6	0.10	0.45	0.13	0.47
	ON	334	371	377	168	−2.9	−0.3	−0.9	+2.4	0.01	0.58	0.15	0.36

variability between 1998 and 2015 is examined in these regions.

3.1.1. Eastern Bay (EB). The SST in the EB region showed typical seasonal variability with warmer (>29 °C) during March to June than during other seasons (Fig. 6a). The seasonal amplitude of SST is ~1.5 °C between winter (28.12 °C) and spring (29.62 °C). The low salinity is noticed during September to December and high during May to June (Fig. 6b). Seasonal amplitude of SSS is 1.4 between fall (30.5) and spring monsoons (31.92). Higher Chl-a is observed during transition between low to high (January-February) and high to low (June to September) and also associating with increase and decrease in salinity. Seasonal mean Chl-a did not show significant variability (Fig. 6c). AOD varied between 0.25 and 0.41 and higher during spring (0.36) and lower during fall (0.27) (Fig. 6d). Lower pH is observed during January and February followed by June to August compared to other months. Lower pH is observed during winter (8.08) and higher during spring (8.13) (Fig. 6e). Lower pCO_2 is observed during spring (328 μatm) and higher during winter (377 μatm) and Summer (362 μatm) (Fig. 6f; Table 2).

Perennial increase in pH is observed during all seasons (+0.0018 to +0.0028 y^{-1}) with high significance (90–95%) (Table 2). The rate of increase in pH is relatively higher during fall and lower during winter. Significant rate of decrease in pCO_2 is noticed during all seasons with higher decrease during fall (−2.9 μatm y^{-1}) and lower in winter (−1.9 μatm y^{-1}; Table 2). Except in fall season, the rate of increase (decrease) in pH (pCO_2) is associated with decrease in Chl-a, SSS and increase in SST (Table 2).

3.1.2. Western Bay (WB). Variability in SST in the WB region is almost similar to that in the EB but higher cooling is noticed during winter than EB (Fig. 6g). The secondary peak in SST is noticed during October in WB, which occurred during November in EB. The seasonal amplitude of SST is ~2.0 °C between winter (26.81 °C) and spring (29.01 °C). The monthly variability in SSS is completely different in the WB with high during January-February and August-September and low in October. Seasonal amplitude of SSS is low (~0.2) between spring (33.18) and summer (33.30) (Fig. 6h). Single peak in Chl-a is observed during June to September compared to other months with low during spring (0.16 mg m^{-3}) and high during winter (0.25 mg m^{-3}) (Fig. 6i). High Chl-a

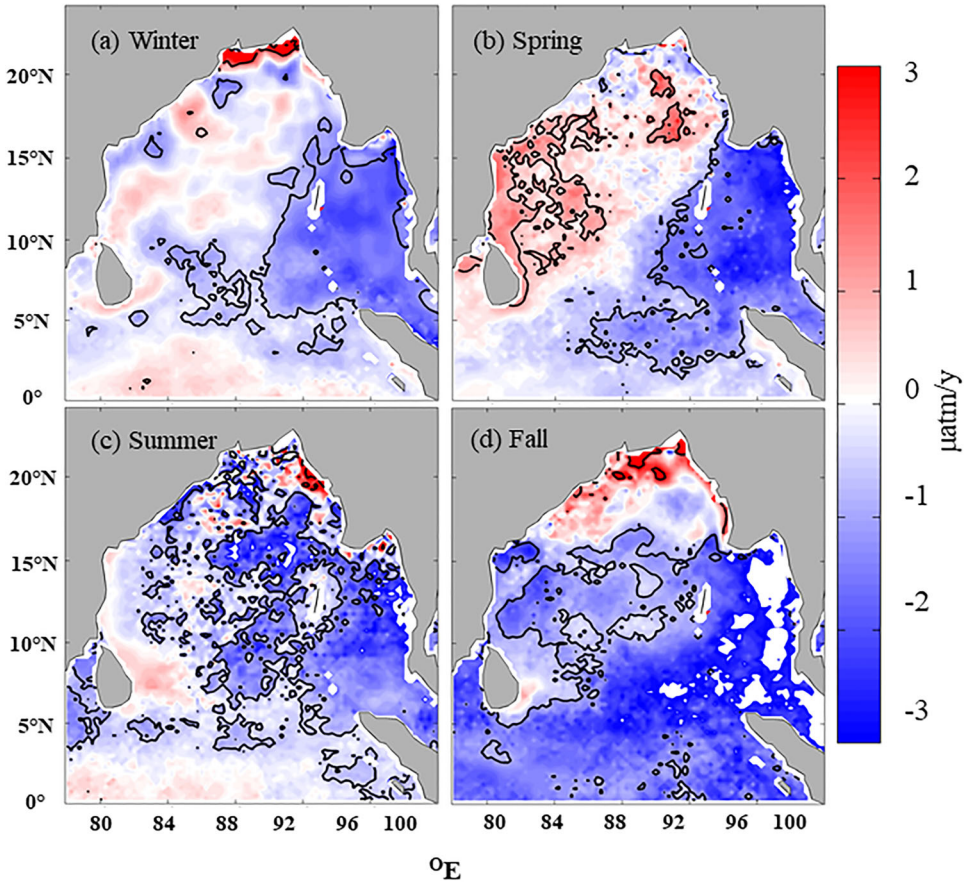

Fig. 5. Seasonal mean rate of increase (positive) or decrease (negative) of pCO_2 (µatm) during (a) winter, (b) spring, (c) summer and (d) fall monsoons in the Bay of Bengal. The region within the thick contour lines shows 90% significant level.

during summer is associated with transition of SSS from low to high and cooling of temperature and increase in AOD. The seasonal mean Chl-a did not show significant variability, except in spring (Table 2). AOD varied between 0.41 and 0.59 and higher during April to June (0.58) and low during January-February and October-November (Fig. 6j). Lower pH is observed during January to February and higher during April to May compared to other months (Fig. 6k). The lower pH is observed during winter (7.99) and higher during fall (8.09) (Fig. 6k; Table 2) associating with warming of surface, increase in AOD and Chl-a. Lower pCO_2 is observed during spring and higher during winter (Fig. 6l).

Decrease in pH is observed during winter and spring ($-0.001\,y^{-1}$) and increase of similar magnitude during summer and fall ($+0.001\,y^{-1}$) (Table 2). The significant rate of increase in pCO_2 is noticed during winter (+0.1 to +0.7 µatm y^{-1}) and decreased during summer and fall (−0.3 and −0.7 µatm y^{-1}). The rate of changes in pH is significant at 80% during all seasons except fall when it was not significant (Table 2).

3.1.3. Central Bay (CB). In the CB, intra-annual variability in SST followed to that of EB and WB with peak during spring and low during winter (Fig. 6m). The seasonal amplitude of SST is ∼2 °C with between winter (27.11 °C) and spring (29.01 °C). The seasonal amplitude of SSS is high (∼0.7) between winter (32.39) and summer (32.98; Fig. 6n). Peak in Chl-a is observed during January and August associated with low and high salinity respectively (Fig. 6o). The high AOD is noticed during summer and the least during fall (Fig. 6p). Lower pH is observed during winter followed by summer compared to other seasons. Lower pH is observed during winter and summer (8.01–8.07) and higher during spring (8.09; Fig. 6q) associating with warming of surface, decrease in AOD and Chl-a. Lower pCO_2 is observed during spring (368 µatm) and higher during winter (447 µatm) (Fig. 6r).

In the CB region, pH and pCO_2 data are collected in BOBOA buoy, deployed at 15°N and 90°E (Sutton et al., 2017). In order to compare the estimated pH and pCO_2 with that of measured, the monthly mean measured data at BOBOA is compared with model derived data during

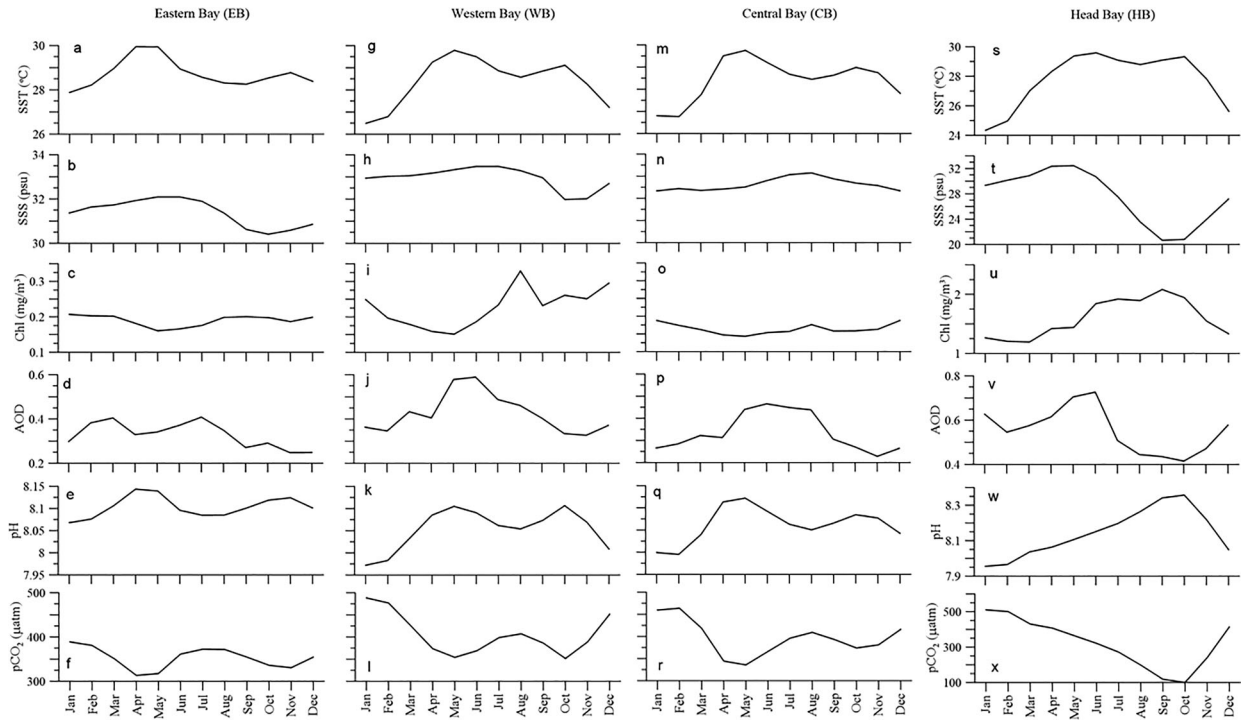

Fig. 6. Mean concentrations of SST, SSS, Chl-a, AOD, and derived pH, and pCO_2 from MLR model (Eqs. (1) and (2)) in the EB, WB, CB and HB regions.

2013–2015, within period of our study, in Fig. S6, supplementary material. The pattern of temperature and salinity between monthly mean measured and satellite data were close to each other. The estimated pH and pCO_2 were deviated from measured with root mean square error (RMSE) of ±0.015 and ±16 µatm respectively. Furthermore, pH and pCO_2 were computed along the I09 transect of World Ocean Circulation Experiment Repeat Hydrography program during 2016, and GEOTRACES cruise data during 2015 (Fig. S7, supplementary material). These data were not used to construct the multiple regression equations. The comparison of the measured and estimated pH revealed the RMSE ±0.018 and 15 µatm for pH and pCO_2 respectively (Fig. S7, supplementary material).

Increase in pH is observed during all seasons (+0.0001 to $+0.0019\,y^{-1}$) however significance (>80%) in variability is noticed during summer and fall monsoons and low significance is noticed during other seasons (Table 2). Similarly, significant rate of decrease in pCO_2 is noticed during summer and fall monsoons (−1.9 and −0.9 µatm y^{-1}) and it is less significant during winter and spring (Table 2).

3.1.4. Head Bay (HB). The intra-annual variability in SST in the HB is different from that of other regions of BoB with cooling during January-February and December and warming during other periods. The highest seasonal amplitude of SST (>4 °C) is noticed between winter (24.97 °C) and summer (29.14 °C; Fig. 6s). The least salinity is noticed throughout the year and varied between 20 and 32 with low during fall and high during spring (Fig. 6t). The seasonal amplitude of SSS varied between fall monsoon (22.38) and spring (31.90). Chl-a displayed single peak associating with low salinity (Fig. 6u). The highest AOD is noticed during spring and the least during summer and fall (Fig. 6v). The lower pH is observed during winter (7.99) and higher during fall monsoon (8.29) and high pH associating with low salinity and AOD (Fig. 6w). Lower pCO_2 is observed during fall (168 µatm) and higher during winter (472 µatm) (Fig. 6x).

Increase in pH is observed during summer ($+0.0014\,y^{-1}$) whereas decreased during other seasons (−0.0002 to $-0.0025\,y^{-1}$) (Table 2). Variability in pH is significant only during fall monsoon than other seasons. Significant rate of decrease in pCO_2 is noticed during spring and summer (−0.2 to −1.6 µatm y^{-1}) whereas increased during winter (+1.3 µatm y^{-1}) and fall (+2.4 µatm y^{-1}) (Table 2).

4. Discussion

4.1. Warming and freshening of the BoB

The annual variation in SST in the BoB exhibited bimodal character (Colborn, 1975) with cooling during

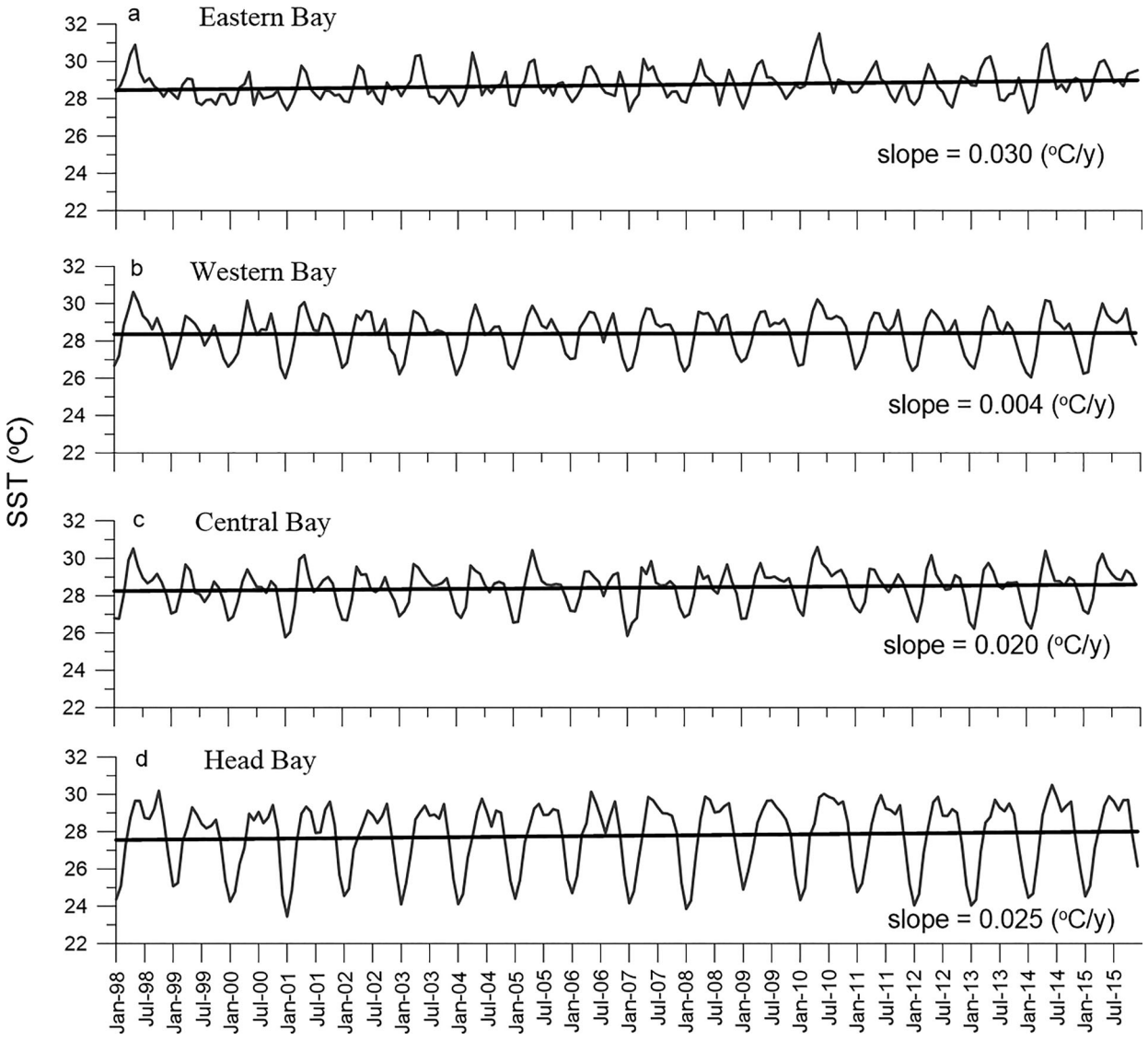

Fig. 7. Variability in monthly mean SST in the (a) Eastern Bay, (b) Western Bay, (c) Central Bay and (d) Head Bay between 1998 and 2015. The rate of change in SST is given in each figure.

winter and summer seasons and warming during the spring and fall seasons - the monsoon transition periods (Fig. S8, supplementary material). Except during winter season in the northern Bay, SST is $> 28\,^{\circ}C$, which is the threshold temperature for the atmospheric deep convection (Gadgil et al., 1984; Shenoi et al., 2002). In contrast, the cold and dry continental winds, blowing from the Siberian region, during winter leads to lower SSTs over the northern BoB (Colborn, 1975; Rao and Sastry, 1981; Shetye et al., 1996). The long-term variability (1998–2015) in SST in the EB and HB was higher (0.03 and $0.025\,^{\circ}C\ y^{-1}$ respectively; Fig. 7a and 7d) and the least warming was noticed in the WB ($0.004\,^{\circ}C\ y^{-1}$; Fig. 7b). Dinesh Kumar et al. (2016) compared long term trends in SST over the Arabian Sea and BoB and they noticed that both the basins experienced warming at almost same rate ($0.012\,^{\circ}C\ y^{-1}$) during the period of 1960–2009. Similarly, the annual mean SST warming rate in the BoB is $0.02 \pm 0.18\,^{\circ}C\ y^{-1}$ over a period of 1998–2015 (Fig. S2, supplementary material). The rate of warming is higher during fall season followed by summer season. Ramanathan et al. (2001) observed a decrease in lower atmospheric temperature and SST due to increased aerosol loading from Indo-Gangetic Plan and the latter is termed as the Asian Brown Cloud (ABC). Sarma et al. (2015) reported decrease in SST and surface air temperature between 1991 and 2011 from December to March in the northern BoB due to increase in atmospheric aerosols

loading. The continental outflow dominates during winter and spring seasons with a significant impact on the radiative forcing over the BoB (Jayaraman et al., 1998; Ramanathan et al., 2001; Satheesh, 2002; Sarma et al., 2015). Increase in AOD over the BoB between 1998 and 2015 is observed in the western and northern BoB due to rapid increase in industrialization (Fig. S5, supplementary material). Paul (2018) analyzed the long-term variability of SST in the BoB in three regions (northern, central and southern BoB) and reported cooling trend over the northern BoB ($-0.02\,^{\circ}C\ y^{-1}$) and warming trend in the central ($+0.01\,^{\circ}C\ y^{-1}$) and southern BoB ($+0.014\,^{\circ}C\ y^{-1}$) over the period of 1980–2014. Our present results are consistent with Paul (2018), but lower than Dinesh Kumar et al. (2016). This study further suggests that rate of warming is increased in the recent decades (1998–2015) compared to previous decades (1980–1998).

The BoB is occupied with freshwater in the upper few tens of meters throughout the year due to river runoff from major riverine systems, such as Ganges-Brahmaputra and Irrawaddy-Salween, and rainfall during the summer and winter seasons (Shetye et al., 1996; Varkey et al., 1996; Vinayachandran et al., 2002; Sengupta et al., 2006; Papa et al., 2010; Paul, 2018). The decrease in salinity is noticed during all seasons in the western, northern and eastern Bay and increase in the central and southern Bay (Fig. S3, supplementary material; Table 2). During winter, the radiated Rossby waves carry low saline water towards the southwestern direction and forms an anticyclonic gyre in the northern BoB (Shankar et al., 2002; Sreenivas et al., 2012). Under the international research efforts of Air-Sea Interactions Research Initiative (ASIRI) in the BoB, salinity measurements carried out using different kinds of instrumentation revealed that SSS in the northern BoB falls to as low as 25 psu and this low salinity layer extends to a depth of ~20 m (Weller et al., 2016). It is further observed that the salinity increases towards central and southern BoB during the summer monsoon (Wijesekera et al., 2016) and it is in agreement with the present results. Trott et al. (2019) analyzed the SODA re-analyzed salinity data over the period of 1993 to 2014 and reported that there is a notable decadal variability in salinity over the BoB. Using same salinity data, Dinesh Kumar et al. (2016) reported an increase in salinity from 1940 to 1972 whereas a decrease from 1973 to 2008 in the BoB. The decrease in salinity trend is well agreed with an increasing trend of precipitation (P) minus Evaporation (E) (Dinesh Kumar et al., 2016; Mukherjee et al., 2018). Therefore, the present results of decreasing salinity trends of $0.01–0.05\,yr^{-1}$ in the HB and EB (Table 2) are consistent with the recent studies (Dinesh Kumar et al., 2016; Mukherjee et al., 2018). The Ganga-Brahmaputra riverine system is originated in the Himalayas where the precipitation stored in the form of snow that is the major freshwater source to the BoB. The IPCC (2013) also reported that the average lower atmospheric temperature is increased by $0.85\,^{\circ}C$ since 1860 over India whereas the Global temperatures are increased by $0.6 \pm 0.2\,^{\circ}C$ since 1990 (Lozan et al., 2001). This may be the prime reason for increase in the retreating of Himalayan glaciers which contributes to the decrease in salinity in the BoB (Roxy et al., 2015a; Paul, 2018). Recently Goes et al. (2020) found that decrease in ice cover in the Himalayan mountains since past three decades associating with increase in atmospheric temperature. An increase in river discharge from the Ganges and Brahmaputra is noticed between 1993 and 2011 (Papa et al., 2012). Trott et al. (2019) also reported increase in freshwater flux into the BoB over the period of 1955 to 1995, which has a significant impact on the distribution of salinity and stratification in the BoB. Intensifying the monsoonal rainfall is also observed in the northern hemisphere between 1850 and 2005 in the CMIP5 models due to an increase in SST (Lee and Wang, 2014). Recently, Dandapat et al. (2020) studied impact of excess and deficit river runoff on the upper ocean characteristics in the BoB between 1965 and 2016 and noticed that strong cooling is observed over the freshwater plume and excess freshwater amplified the EICC during excess river discharge period. In contrast, more heat accumulated in the upper 100 m of plume area during deficit river runoff years suggesting that magnitude of freshwater discharge has significant impact on upper ocean processes. Therefore, the observed l decreasing trend in SSS in the BoB between 1998 and 2015 may be combined result of increasing trends in river discharge and precipitation.

The change in the freshwater flux and SST has a significant impact on altering the BoB stratification and air-sea interaction processes (Shenoi et al., 2002; Sengupta et al., 2006; Neetu et al., 2012). This leads to decrease of nutrients' input from subsurface resulting in decrease in primary productivity. In contrast, Behrenfeld et al. (2006) studied climate driven trends in primary production and noticed anomalous cooling associated with decrease in net primary production in the BoB. Roxy et al. (2015a) found that about 20% decrease in phytoplankton biomass associating with warming and stratification in the western Indian Ocean. Warming also influences solubility in gas that brings changes in pH and pCO_2 levels in the upper ocean. In addition to this, stratification decreases input of DIC and pCO_2 rich waters from the subsurface and river discharge decreased DIC and pCO_2 but increases pH.

4.2. Long-term variations in surface water pH and pCO_2 in the BoB

The pH and pCO_2 in the BoB shows strong salinity influence as the freshwater from the Ganges is relatively basic

and undersaturated than seawater (Kumar et al., 1996; Sarma et al., 2012a, 2012b). Mukhopadhyay et al. (2002) studied pH and pCO_2 at the Hooghly (Ganges) estuary and noticed higher pH and under-saturation of pCO_2 during peak discharge (summer) period and contrasting to that is noticed during non-monsoon period. Due to huge discharge (>25,000 m^3 s^{-1}), the impact of pollution will be diluted during monsoon resulting in preserving the source water characteristics (high pH and low pCO_2) during monsoon and weakening of discharge during non-monsoon period accumulates significant amount of atmospheric deposition of pollutants leading to low pH and high pCO_2 (Mukhopadhyay et al., 2002). Sarma et al. (2012a) found high pH in the northwestern coastal Bay where high freshwater discharge from the Ganges occurred and contrasting to that occurred in the southwestern coastal Bay where freshwater discharge from monsoonal rivers lead to low pH (Sarma et al., 2011, 2012a, 2012b). Such differences are caused by source of freshwater as the monsoonal rivers receive freshwater through precipitation. Since the rain water pH is as low as 5.5 to 6.5, and significant bacterial decomposition of organic matter occurs in the en-route river water from upper reaches to the estuary leading to low pH (Sarma et al., 2011). In addition to this, the flow of water is an order of magnitude less in the peninsular rivers (<1000 m^3 s^{-1}) than Ganges (>25000 m^3 s^{-1}). The eastern BoB and Andaman Sea is influenced discharge from Irrawady-Salween river systems whereas Western Bay is influenced by peninsular and Ganges and head Bay is influenced solely by Ganges. In the case of central Bay, the mixture of different source of river is expected to influence. Hence the BoB is divided into four regions and their influence is discussed.

4.2.1. Long-term variability in pH and pCO_2 in the Eastern Bay (EB). The estimated rate of pH (pCO_2) in the EB showed increasing trend at the rate of +0.0018 to +0.0028/y (−1.9 to −2.9 µatm y^{-1}) associating with decrease in salinity (−0.01 to −0.04 y^{-1}) and increase in SST (0.02 to 0.04 °C y^{-1}; Table 2). The EB region is influenced mainly by discharge from Irrawady and Salween river systems (Varkey et al., 1996). The raise in temperature is a manifestation of stratification driven by freshwater discharge in the BoB (Trott et al., 2019; Dandapat et al., 2020). Based on Eq. (1), the changes in SST and SSS increases pH by 73% and 27% respectively and decreases pCO_2 by similar magnitude in the EB. Since the increase in SST is caused by salinity stratification, the impact of SST on pH is indirectly caused by SSS. Though warming of waters decreases solubility of water, however, decrease in SSS resulting in high pH and low pCO_2 dominant the impact of solubility. This leads to net increase in pH and decrease in pCO_2 in the EB (Figs. 4 and 5; Table 2). The rate and area of warming in the EB increased from winter to fall monsoon (Fig. S2, supplementary material) due to spread of low saline water (Fig. S3, supplementary material) leading perennial increase in pH during all seasons in the EB (Fig. 4).

4.2.2. Long-term variability in pH and pCO_2 in the Western Bay (WB). The variability temperature data between 1998 and 2015 in the WB shows that cooling at the rate of −0.011 to 0.015 °C y^{-1} associating with freshening at the rate of −0.017 to −0.018 y^{-1} (Table 2; Figs. S2 and S3) during winter and spring season. Based on the observed negative relationship of salinity with pH, decrease in salinity should increase pH as shown in other regions in the BoB. In contrast, pH (pCO_2) decreased (increased) at the rate of −0.001 y^{-1} (+0.1 to +0.7 µatm y^{-1}) during winter and spring associating with decreasing rate of salinity suggests that other than local oceanographic processes may be responsible for decrease in SST and pH in the WB. Ramanathan et al. (2001) found that decrease in atmospheric temperature associated with Asian Brown Cloud, forms due to large amounts of aerosols (such as soot and dust) produced in the combustion of fossil fuels and biomass, in the northern BoB. Enhanced atmospheric dust was reported earlier over the BoB during winter when winds bring secondary pollutants from the Indo-Gangetic Plain (Zhang and Reid, 2010). High concentrations of sulfates and nitrates were reported in the atmospheric dust collected over the BoB compared other regions in the world (Kumar et al., 2008). Sarma et al. (2015) showed that decrease in surface air temperature and SST in the northern BoB during winter and spring seasons are due to increase in atmospheric dust between 1991 and 2011. Based on decade-long time-series observations (2000–2009), Zhang and Reid (2010) reported that the rate of increase in AOD over the BoB is the highest (0.007 y^{-1}) than elsewhere in the world (0.002 y^{-1}). The present study also reports high rate of increase in AOD (0.008 to 0.009 y^{-1}) in the WB during winter and spring. Moreover, higher rate of increase in AOD in the northwestern BoB during winter and spring seasons (Fig. S5, supplementary material) are associated with decrease in SST (Fig. S2, supplementary material) whereas lower AOD was observed in the southern BoB during summer is associating with increase in SST. The difference between AOD during winter/spring and summer is not from the same source due to seasonal reversal of the winds and therefore their concentrations and impacts are expected to be different on the SST (Kumar et al., 2008; Srinivas et al., 2011). However, the magnitude of decrease in SST is relatively smaller during summer than winter as the former period receives primary

(natural) aerosols, mainly marine, and the latter period received secondary (anthropogenic) aerosols from terrestrial sources (Kumar et al., 2008). Sarma et al. (2015) found that decrease in pH by $0.007\,y^{-1}$ during spring between 1991 and 2011 is attributed to deposition of atmospheric pollutants in the western coastal BoB. Despite decrease in SSS in the western BoB during winter/spring, which is expected to increase pH (Figs. 4 and S3), however, decreasing trends in pH may mainly be caused by decreased SST due to increase in atmospheric dust deposition. In contrast, increase (decrease) in pH (pCO_2) at the rate of $+0.001\,y^{-1}$ (-0.3 to -0.7 μatm y^{-1}) was observed during summer and fall monsoons in the WB. This study suggests that deposition of atmospheric dust (pollutants) in the WB decreases pH and increases pCO_2 during winter and spring seasons and contrasting to that occurs during summer and fall due to variable source of dust (continental versus marine origin).

4.2.3. Long-term variations in pH and pCO_2 in the Central Bay (CB). The variability temperature data between 1998 and 2015 in the CB region shows that warming at the rate of $+0.01$ to $+0.025\,°C\ y^{-1}$ associating with slight increase in SSS during winter ($+0.02\,y^{-1}$) and significant modifications were not observed during other seasons (Table 2). Variability in pH (pCO_2) between 1998 and 2015 suggests that increase (decrease) by $+0.0001$ to $+0.0019\,y^{-1}$ (-0.01 to -1.9 μatm y^{-1}) in the CB region and the variations are significant only during summer and fall monsoons. Since the CB region is away from the land, the impact of atmospheric dust is low as evidenced from that very low rate of increase in AOD (0.0015 to $0.0066\,y^{-1}$) (Fig. S5). The increase (decrease) in pH (pCO_2) is mainly associated with significant warming of surface waters during summer and fall monsoon seasons (Table 2). The southward advection of low saline waters from the Ganges-Brahmaputra discharge (Fig. S9) influences significantly the CB region resulting in high (low) pH (pCO_2).

4.2.4. Long-term variations in pH and pCO_2 in the head Bay (HB). The variations temperature data between 1998 and 2015 in the HB shows significant warming during spring and summer monsoons and cooling during fall associating with significant decrease in salinity (Figs. 2 and 3, supplementary material). Since HB is situated close to the Ganges-Brahmaputra river discharge region, and also close to land, the influence of both river discharge and atmospheric pollution is expected to be high. The rate of increase in AOD is the highest (0.01 to $0.018\,y^{-1}$) among other regions with especially higher during winter and fall monsoon period (Table 2). Despite HB region received high amount of freshwater, as evidenced from salinity distribution (Fig. S9, supplementary material), decrease (increase) in pH (pCO_2) was noticed during winter and fall monsoon associating with higher increase in AOD, SST and SSS and contrasting to that is observed during spring and summer suggesting that warming, decrease in freshwater discharge and atmospheric deposition contribute to decrease (increase) in pH (pCO_2) in the HB.

4.2.5. Comparison of pH trends by different models and present study. Bopp et al. (2013) compared simulations performed under the framework of Coupled Model Inter Comparison Project 5 (CMICP5) on stressors of ocean ecosystem in the 21st century. The 10 Earth system models used in this comparison showed similar trends in ocean warming and acidification over the 21st century. Under the "business as-usual" scenario RCP8.5, the annual change in SST and surface pH is $+0.0273 \pm 0.0072\,°C\ y^{-1}$ and $-0.0033 \pm 0.0003\ y^{-1}$ between 1990 and 2090, respectively, in the global ocean. Bopp et al. (2013) further found that SST and pH projections are robust across models. As per our model (Eq. (1)), the increase in SST by $+0.0273\,°C\ y^{-1}$ would increase pH by $+0.0012\,y^{-1}$ at constant salinity. In contrast, all models projected uniform decrease in pH in the entire Indian Ocean. Lauvset et al. (2015), based on SOCAT data, projected that the long-term decrease in pH by $-0.0024 \pm 0.0004\ y^{-1}$ between 1981 and 2011 whereas $-0.0027 \pm 0.0005\ y^{-1}$ between 1991 and 2011 in the Indian Ocean biome (north of 35°S). Jiang et al. (2019) predicted the decrease in pH in the global ocean including in the BoB. They further predicted that decrease in pH is at higher rates in the northern than southern latitudes, which are at present sink for atmospheric CO_2 and these regions may experience the most important pH-associated increase of seawater pCO_2. Therefore, it is expected that global sea-air CO_2 fluxes may likely undergo important changes during the 21st century.

The global models have taken BoB is more acidic (8.05) than Arabian Sea (8.1) (Bopp et al., 2013). In contrast, observations indicate Arabian Sea is more acidic than BoB (Kumar et al., 1996; Sarma et al., 1998, 2012a, 2015; Jiang et al., 2019) due to significant input of freshwater discharge with high pH into the latter, and high vertical mixing resulting in injection of low pH subsurface waters to surface in the former basin (e.g. Goyet et al., 1998; Sarma et al., 1998). Due to lack of seasonal and spatial pH data in the climatology, and extrapolation of limited data led to large errors in the pH used by models. In addition to this, since global models do not include inter-annual variations in the river discharge, they will not project the impact of variations in river discharge on

Table 3. Comparison of climatological mean pH and pCO_2 estimated by different models in selected regions in the Bay of Bengal.

Region	Season	Takahashi	SOCAT	Present study	Lauvset et al. (2015)	Present study
			pCO_2 (μatm)		pH	
Northern BoB (85–90°E; 14–18°N)	DJF	342	347 ± 2	440 ± 15	8.095 ± 0.027	8.018 ± 0.015
	MAM	347	357 ± 2	391 ± 11	8.040 ± 0.007	8.006 ± 0.010
	JJAS	351	356 ± 2	367 ± 13	8.052 ± 0.011	8.091 ± 0.013
	ON	348	355 ± 2	365 ± 18	8.054 ± 0.001	8.092 ± 0.018
Western BoB (80–85°E; 10–14°N)	DJF	352	354 ± 2	447 ± 7	NaN	8.013 ± 0.008
	MAM	356	365 ± 3	402 ± 10	NaN	8.016 ± 0.010
	JJAS	356	363 ± 1	365 ± 13	NaN	8.094 ± 0.012
	ON	353	358 ± 1	377 ± 15	NaN	8.081 ± 0.015
Southern BoB (85–90°E; 2–6°N)	DJF	360	366 ± 1	439 ± 4	NaN	8.022 ± 0.004
	MAM	369	372 ± 1	366 ± 8	8.055 ± 0.009	8.094 ± 0.008
	JJAS	366	370 ± 2	403 ± 12	8.069 ± 0.003	8.057 ± 0.011
	ON	361	366 ± 2	433 ± 12	NaN	8.028 ± 0.011
Eastern BoB (90–95°E; 6–10°N)	DJF	359	358 ± 2	434 ± 7	8.076 ± 0.005	8.025 ± 0.006
	MAM	360	369 ± 1	369 ± 15	NaN	8.112 ± 0.015
	JJAS	359	362 ± 2	387 ± 16	NaN	8.072 ± 0.015
	ON	353	354 ± 2	429 ± 11	8.097 ± 0.003	8.030 ± 0.011

NaN denotes no data available (Takahashi et al., 2014; Bakker et al., 2016; Lauvset et al., 2015). The reference year for both pCO_2 climatology and present study are 2005.

the biogeochemical properties. Doney et al. (2007) found that atmospheric deposition is highly important in the BoB and South China Sea, but its impact may be negligible in other parts of global ocean. Hence, global models did not include atmospheric chemistry and their deposition into the surface ocean while predicting the surface ocean pH. These could be the possible reasons for the projected decrease in pH in the BoB by global models.

Despite the observed trends in surface water pH at Hawaii Ocean Time-Series (HOTS) and Bermuda Atlantic Time-Series (BATS) locations suggest a decrease by $-0.0014\,y^{-1}$ (Bates et al., 2014), our study suggests an increase at the rate of $+0.0005$ to $+0.003\,y^{-1}$ in the entire BoB, except in the western Bay, where a decrease in pH by -0.0005 to $-0.0015\,y^{-1}$ is noticed during winter and spring seasons (Fig. 4a and 4b). The annual mean pH shows increasing trend of $+0.001\,y^{-1}$ in the entire BoB and it is contrasting to that of global models and observations elsewhere in the world.

Similarly, the observed trends in surface water pCO_2 at HOTS, BATS and South Indian Ocean time-series (Metzl, 2009) locations suggest an increase in pCO_2 by $+1.2$ to $+1.6$ μtam y^{-1} and several model predictions also estimated close this rate (Bopp et al., 2013). For instance, Lauvset et al. (2015) estimated increase in pCO_2 by $+1.49 \pm 0.25$ and $+1.55 \pm 0.26$ μatm y^{-1} between 1981–2011 and 1991–2011 in the Indian Ocean (north of 35°S). Similarly, Tjiputra et al. (2014) found the pCO_2 increase by $+1.5$ μatm y^{-1} in the northern Indian Ocean between 1970 and 2011 whereas this increase is expected to be $+8$ to 9 μatm y^{-1} between 2060 and 2100. Such a large increase in pCO_2 is estimated to be caused by increase in DIC followed by temperature increase. On the other hand, the impact of SSS is estimated to be small, i.e. -0.2 μatm y^{-1} during 1970–2011 and -0.4 μatm y^{-1} during 2060–2100 (Tjiputra et al., 2014). On the contrary, the estimated pCO_2 trend in the present study suggests that increase in pCO_2 from $+0$ to $+0.8$ μatm y^{-1} during November to May in the western BoB with a maximum increase during February to April, and decrease in pCO_2 from 0 to -2 μatm y^{-1} during other periods in the entire BoB.

We compared here pCO_2 and pH based on Takahashi et al. (2009; Takahashi et al., 2014) and SOCAT climatology (Lauvset et al., 2015). The climatological pCO_2 and pH at selected regions are compared with present MLR model in Table 3. Both pCO_2 and pH derived by present study is well associated with SOCAT and Takahashi climatology during most of the periods, however, significant deviations are noticed during winter and spring monsoons. Significantly higher pCO_2 and low pH were noticed during winter and spring in the northern and western BoB whereas southern and eastern BoB during winter only (Table 3). Relatively high pCO_2 and lower pH were noticed in the present study compared to SOCAT and Takahashi climatology during all seasons, except in spring, in the southern BoB (Table 3). The seasonal amplitude of pCO_2 as high as 60 μatm was measured in the central Bay by BOBOA buoy. In contrast, the amplitude of seasonal variability was 9, 3, 9 and 7 μatm

in the northern, western, southern and eastern BoB respectively in the Takahashi climatology whereas it was 10, 11, 6 and 15 μatm respectively in the SOCAT climatology. In contrast, the seasonal amplitude is higher (75, 82, 73 and 65 μatm respectively) in the northern, western, southern and eastern BoB (Table 3) and it is close to that of measured. The high seasonal amplitude is mainly caused by seasonal reversal in the wind direction, upper ocean circulation, mixing and also seasonal variability in magnitude of river discharge. Due to lack of seasonal data and weak spatial coverage, the large seasonal variability could not be captured in both SOCAT and Takahashi climatology. In addition to this, the present model captured the influence of atmospheric deposition, influence of river discharge and spatial variability seems to be well resolved.

The present study indicates that both river discharge and deposition of atmospheric pollutants are the dominant controlling factors on pH and pCO_2 in surface waters. None of the global models do not include inter-annual variation in the river discharge, and atmospheric deposition resulting in poor simulation of surface pCO_2 in the BoB (Aumont and Bopp, 2006; Matear and Lenton, 2008; Le Quere et al., 2008; Thomas et al., 2008; Graven et al., 2012). Since BoB is covered by land mass on three directions, and >30% of world population is dwelling along its coast, rapid increase in atmospheric dust due to industrialization (Srinivas and Sarin, 2013; Yadav et al., 2016, 2020) would influence on pH and pCO_2 dynamics in the BoB. Sarma et al. (2013) compared the pCO_2 simulations of various the global models, which were used in IPCC Reports. It is noticed that none of the global models could simulate neither seasonality in pCO_2 nor long-term variability in the BoB and it is attributed to weak vertical mixing, lack of inter-annual variability of river discharge and atmospheric pollutants deposition. The present model suggests that inclusion of such processes improves seasonality and spatial variability in pH and pCO_2 in the BoB.

5. Summary and conclusions

In order to examine the variability in ocean acidification (OA) and pCO_2 levels between 1998 and 2015 in the BoB region, the multiple linear regression (MLR) equations were developed based on pH and pCO_2 data collected between 1991 and 2019. Using remote sensing SST, Chl-a and modelled SSS data, pH and pCO_2 are estimated using MLR equations between 1998 and 2015 in the Bay of Bengal (BoB). The results suggested that entire BoB is warming at the rate of 0.004 to 0.03 °C y^{-1} with strong seasonal and regional variability. Relatively higher warming was noticed during summer and fall monsoon than winter and spring monsoons. In contrast, cooling of western BoB is noticed during winter and spring associated with increase in atmospheric dust content, as evidenced from increase in Aerosol Optical Depth (AOD), suggesting that enhanced atmospheric dust inhibited solar radiation to the lower atmosphere resulting in decrease in SST. Decrease in salinity is noticed in the eastern and northwestern BoB throughout the year whereas it was increased in the southern BoB due to increase of melting of Himalayan ice cover due to increase in atmospheric temperature resulting in increase in discharge. Decrease in Chl-a is noticed in the entire BoB due to increase in stratification associating with decrease in salinity. Increase in pH is observed in the eastern and southern Bay during all seasons associating with warming and decrease in salinity suggests that enhanced freshwater inputs with high pH enhanced pH in the BoB. Decrease in pH and increase in pCO_2 is noticed in the western Bay associated with cooling and increase in AOD suggesting that deposition of atmospheric pollutants decreased pH. Increase in pH and decrease in pCO_2 is noticed during all seasons in the eastern and central Bay associating with decrease in salinity. Decrease in pH and increase in pCO_2 is observed in the head Bay associating with atmospheric input of pollutants. This study suggests that change in freshwater input to the BoB caused by increase in atmospheric temperature leading to melting of Himalayan ice cover/freshwater flux that increased pH and decreased pCO_2 levels resulting in stronger sink for the atmospheric CO_2 in the recent years.

The BOBOA buoy made continuous pCO_2 measurements in the central Bay and found the seasonal amplitude of 60 μatm of pCO_2. In contrast, both Takahashi (<10 μatm) and SOCAT (<15 μatm) climatologies underestimated seasonal amplitude due to lack of seasonal and spatial data. Our present study suggests that the high amplitude of seasonal variability by >60 μatm, close to that of measured, is driven by seasonal variability in freshwater inputs and atmospheric deposition of pollutants. Since these two processes are not part of the global models, such large seasonal variability in pCO_2 is not reproduced. These problems are not alone to the BoB but also in the coastal regions where river discharge and human impact through atmospheric deposition is more likely. Since these two processes have only regional importance, it may be possible initially to incorporate in the regional models, such as discussed in Joshi et al. (2020), for better understanding of influence of human-impact on ocean acidification and sea-to-air fluxes of CO_2 in future.

Acknowledgements

We would like to thank Director, CSIR-National Institute of Oceanography for his encouragement and

support. We appreciate the NOAA for making available satellite data to conduct this work. We would like to thank WOCE repeat hydrography group for making available their data of transect I09N and I01E for this study. We appreciate for making available Bay of Bengal Ocean Acidification (BOBOA) Mooring data for calibration of our modeled data. We appreciate Dr. Siv Lauvset, Bjerknes Centre for Climate Research, Norway for sharing SOCAT_pH data for the Bay of Bengal. The surface Ocean CO_2 Atlas (SOCAT; www.socat.info) is an international effort, endorsed by the International Ocean Carbon Coordination Project (IOCCP), the Surface Ocean Lower Atmosphere Study (SOLAS) and the Integrated Marine Biogeochemistry and Ecosystem Research program (IMBER), to deliver a uniformly quality-controlled surface ocean CO_2 data base. We would like to thank SOCAT group for making available climatology data for this study. We would like to thank two anonymous reviewers for significantly improving the presentation of our work. This has NIO contribution number 6794.

Disclosure statement

No potential conflict of interest was reported by the authors.

Supplemental data

Supplemental data for this article is available online at https://doi.org/10.1080/16000889.2021.1971924.

References

Aumont, O. and Bopp, L. 2006. Globalizing results from ocean in situ iron fertilization studies. *Global Biogeochem. Cy.* **20**, GB2017, 1–15.

Bakker, D. C. E., Alin, S. R., Bates, N., Becker, M., Castaño-Primo, R. and co-authors. 2020. *Surface Ocean CO_2 Atlas Database Version 2020 (SOCATv2020)* (NCEI Accession 0210711). NOAA National Centers for Environmental Information. Dataset..

Bakker, D. C. E., Pfeil, B., Landa, C. S., Metzl, N., O'Brien, K. M. and co-authors. 2016. A multi-decade record of high-quality fCO_2 data in version 3 of the Surface Ocean CO_2 Atlas (SOCAT). *Earth Syst. Sci. Data* **8**, 383–413.

Bates, N., Astor, Y. M., Church, M. J., Currie, K., Dore, J. E. and co-authors. 2014. A time-series view of changing surface ocean chemistry due to ocean uptake of anthropogenic CO_2 and Ocean Acidification. *Oceanography* **27**, 126–141.

Behrenfeld, M. J., O'Malley, R. T., Siegel, D. A., McClain, C. R., Sarmiento, J. L. and co-authors. 2006. Climate-driven trends in contemporary ocean productivity. *Nature* **444**, 752–755.

Bopp, L., Resplandy, L., Orr, J. C., Doney, S. C., Dunne, J. P. and co-authors. 2013. Multiple stressors of ocean ecosystems in the 21st century: Projections with CMIP5 models. *Biogeosciences* **10**, 6225–6245.

Cai, W. J., Hu, X., Huang, W. J., Murrell, M. C., Lehrter, J. C. and co-authors. 2011. Acidification of subsurface coastal waters enhanced by eutrophication. *Nature Geosci.* **4**, 766–770.

Cai, W. J., Xu, Y. Y., Feely, R. A., Wanninkhof, R., Jonsson, B. and co-authors. 2020. Controls on surface water carbonate chemistry along North American ocean margins. *Nat. Commun.* **11**, 2691.

Colborn, J. G. 1975. The thermal structure of the Indian Ocean. IIOE Oceanographic Monographs No. **2**, p. 173.

Dandapat, S., Gnanaseelan, C. and Parekh, A. 2020. Impact of excess and deficit river runoff on Bay of Bengal upper ocean characteristics using an ocean general circulation model. *Deep Sea Res. II* **172**, 104714.

Dentener, F., Kinne, S., Bond, T., Boucher, O., Cofala, J. and co-authors. 2006. Emissions of primary aerosol and precursor gases in the years 2000 and 1750, prescribed data-sets for AeroCom. *Atmos. Chem. Phys.* **6**, 4321–4344.

Dinesh Kumar, P. K., Paul, Y. S., Muraleedharan, K. R., Murty, V. S. N. and Preenu, P. N. 2016. Comparison of long-term variability of Sea Surface Temperature in the Arabian Sea and Bay of Bengal. *Reg. Stud. Mar. Sci.* **3**, 67–75.

Dlugokencky, E. and Tans, P. 2020. *Trends in atmospheric carbon dioxide, National Oceanic and Atmospheric Administration*. Earth System Research Laboratory (NOAA/ESRL). http://www.esrl.noaa.gov/gmd/ccgg/trends/global.html.

Doney, S. C. 2010. The growing human footprint on coastal and open-ocean biogeochemistry. *Science* **328**, 1512–1516.

Doney, S. C., Mahowald, N., Lima, I., Feely, R. A., Mackenzie, F. T. and co-authors. 2007. Impact of anthropogenic atmospheric nitrogen and sulfur deposition on ocean acidification and the inorganic carbon system. *Proc. Natl. Acad. Sci. USA* **104**, 14580–14585.

Gadgil, S., Joseph, P. V. and Joshi, N. V. 1984. Ocean–atmosphere coupling over monsoon regions. *Nature* **312**, 141–143.

Goes, J. I., Tian, H., do Rosario Gomes, H., Anderson, O. R., Al-Hashmi, K. and co-authors. 2020. Ecosystem state change in the Arabian Sea fuelled by the recent loss of snow over the Himalayan-Tibetan plateau region. *Sci. Rep.* **10**, 7422–7428.

Goyet, C., Millero, F. J., O'Sullivan, D. W., Eischeid, G., McCue, S. J. and co-authors. 1998. Temporal variations of pCO_2 in surface seawater of the Arabian Sea in 1995. *Deep Sea Res. I* **45**, 609–623.

Grasshoff, K., Ehrhardt, M., Kremling, K. (eds.). 1983. *Methods of Seawater Analysis*. Verlag, Chemie, Weinheim.

Graven, H. D., Gruber, N., Key, R. M., Khatiwala, S. and Giraud, X. 2012. Changing controls on oceanic radiocarbon: New insights on shallow-to-deep ocean exchange and anthropogenic CO_2 uptake. *J. Geophys. Res.* **117,** C10005, 1–16.

Hall, E. R., Wickes, L., Burnett, L. E., Scott, G. I., Hernandez, D. and co-authors. 2020. Acidification in the U.S. Southeast:

Causes, Potential consequences and the role of the southeast ocean and coastal acidification network. *Front. Mar. Sci.* **7**, 1–548.

Howarth, R. W., Billen, G., Swaney, D., Townsend, A., Jaworski, N. and co-authors. 1996. Regional nitrogen budgets and riverine N & P fluxes for the drainages to the North Atlantic Ocean: Natural and human influences. In: *Nitrogen Cycling in the North Atlantic Ocean and Its Watersheds*. Springer, Dordrecht, pp. 75–139.

Howarth, R. W., Boyer, E. W., Pabich, W. J. and Galloway, J. N. 2002. Nitrogen use in the United States from 1961–2000 and potential future trends. *AMBIO* **31**, 88–96.

IPCC. 2013. *Climate Change 2013: The Physical Science Basis. Contribution of Working Group I to the Fifth Assessment Report of the Intergovernmental Panel on Climate Change* (eds. T. F. Stocker, D. Qin, G.-K. Plattner, M. Tignor, S. K. Allen, J. Boschung, A. Nauels, Y. Xia, V. Bex, and P. M. Midgley). Cambridge University Press, Cambridge, UK and New York, NY.

Jayaraman, A., Lubin, D., Ramachandran, S., Ramanathan, V., Woodbridge, E. and co-authors. 1998. Direct observations of aerosol radiative forcing over the tropical Indian Ocean during the January-February 1996 pre-INDOEX cruise. *J. Geophys. Res.* **103**, 13827–13836.

Jiang, L. Q., Carter, B. R., Feely, R. A., Lauvset, S. K. and Olsen, A. 2019. Surface ocean pH and buffer capacity: Past, present and future. *Sci. Rep.* **9**, 18624.

Joos, F. and Spahni, R. 2008. Rates of change in natural and anthropogenic radiative forcing over the past 20,000 years. *Proc. Natl. Acad. Sci. USA* **105**, 1425–1430.

Joshi, A. P., Roy Chowdhury, R., Kumar, V. and Warrior, H. V. 2020. Configuration and skill assessment of the coupled biogeochemical model for the carbonate system in the Bay of Bengal. *Mar. Chem.* **226**, 103871.

Krishna, M. S., Prasad, M. H. K., Rao, D. B., Viswanadham, R., Sarma, V. V. S. S. and co-authors. 2016. Export of dissolved inorganic nutrients to the northern Indian Ocean from the Indian monsoonal rivers during discharge period. *Geochim. Cosmochim. Acta* **172**, 430–443.

Krishna, M. S., Prasad, V. R., Sarma, V. V. S. S., Reddy, N. P. C., Hemalatha, K. P. J. and co-authors. 2015. Fluxes of dissolved organic carbon and nitrogen to the northern Indian Ocean from the Indian monsoonal rivers. *J. Geophys. Res. Biogeosci.* **120**, 2067–2080.

Kumar, M. D., Naqvi, S. W. A., George, M. D. and Jayakumar, D. A. 1996. A sink for atmospheric carbon dioxide in the northeast Indian Ocean. *J. Geophys. Res.* **101**, 18121–18125.

Kumar, A., Sudheer, A. K. and Sarin, M. M. 2008. Chemical characteristics of aerosols in MABL of Bay of Bengal and Arabian Sea during spring inter-monsoon: A comparative study. *J. Earth Syst. Sci.* **117**, 325–332.

Landschutzer, P., Laruelle, G. G., Roobaert, A. and Regnier, P. 2020. A uniform pCO_2 climatology combining open and coastal oceans. *Earth Syst. Sci. Data* **12**, 2537–2553.

Lauvset, S. K., Gruber, N., Landschutzer, P., Olsen, A. and Tjiputra, J. 2015. Trends and drivers in global surface ocean pH over the past 3 decades. *Biogeosciences* **12**, 1285–1298.

Le Quere, C., Ro Denbeck, C., Buitenhuis, E. T., Conway, T. J., Langenfelds, R. and co-authors. 2008. Saturation of the Southern Ocean CO_2 sink due to recent climate change. *Science* **319**, 570–570.

Lee, J. Y. and Wang, B. 2014. Future change of global monsoon in the CMIP5. *Clim. Dyn.* **42**, 101–119.

Lewis, E. and Wallace, D. W. R. 1998. *Ornl/Cdiac-105*. Carbon Dioxide Information Analysis Center, Oak Ridge National Laboratory, US Department of Energy, Oak Ridge, TN.

Lozan, J. L., Grabl, H. and P. Huper. 2001. Summary: Warming signals from climate. In: *Climate of 21st Century: Changes and Risks*. Wissenschaftliche Auswertungen, Berlin, Germany.

Mackenzie, T., Ver, L. M. and Lerman, A. 1995. Modeling the behaviour of biogeochemical cycles in the land-coastal margin system during global change. In International Symposium on Earth Environment, pp. 149–200.

Matear, R. J. and Lenton, A. 2008. Impact of historical climate change on the Southern Ocean carbon cycle. *J. Clim.* **21**, 2820–2834.

Metzl, N. 2009. Decadal increase of oceanic carbon dioxide in Southern Indian Ocean surface waters (1991–2007). *Deep Sea Res. II* **56**, 607–619.

Millero, F. J., Graham, T. B., Huang, F., Bustos-Serrano, H. and Pierrot, D. 2006. Dissociation constants of carbonic acid in seawater as a function of salinity and temperature. *Mar. Chem.* **100**, 80–94.

Mukherjee, S., Aadhar, S., Stone, D. and Mishra, V. 2018. Increase in extreme precipitation events under anthropogenic warming in India. *Weather Clim. Extrem.* **20**, 45–53.

Mukhopadhyay, S. K., Biswas, H., De, T. K., Sen, S. and Jana, T. K. 2002. Seasonal effects on the air-water carbon dioxide exchange in the Hooghly estuary, NE coast of Bay of Bengal, India. *J. Environ. Monit.* **4**, 549–552.

NAPAP. 1991. *Acid Deposition: State of Science and Technology*. National Acid Precipitation Assessment Program Office of the Director, Washington, DC, p. 2053.

Neetu, S., Lengaigne, M., Vincent, E. M., Vialard, J., Madec, G. and co-authors. 2012. Influence of upper-ocean stratification on tropical cyclone-induced surface cooling in the Bay of Bengal. *J. Geophys. Res.* **117,** C12020, 1–19.

Papa, F., Bala, S. K., Pandey, R. K., Durand, F., Gopalakrishna, V. V. and co-authors. 2012. Ganga-Brahmaputra river discharge from Jason-2 radar altimetry: An update to the long-term satellite-derived estimates of continental freshwater forcing flux into the Bay of Bengal. *J. Geophys. Res.* **117,** C11021, 1–13**.**

Papa, F., Durand, F., Rossow, W. B., Rahman, A. and Bala, S. K. 2010. Satellite altimeter-derived monthly discharge of the Ganga-Brahmaputra River and its seasonal to interannual variations from 1993 to 2008. *J. Geophys. Res.* **115,** C12013, 1–19.

Paul, S. 2018. *A study on the impact of Climatic Events induced long-term trends in Sea Surface Temperature and Ganges-Brahmaputra river discharge on the frequency and intensity of*

Tropical Cyclones over the Bay of Bengal. PhD Thesis, Andhra University.

Ramanathan, V., Crutzen, P. J., Kiehl, J. T. and Rosenfeld, D. 2001. Aerosols, climate, and the hydrological cycle. *Science* **294**, 2119–2124.

Rao, D. P. and Sastry, J. S. 1981. Circulation and distribution of some hydrographical properties during the late winter in the Bay of Bengal, Mahasagar. *Bull. Natl. Inst. Oceanogr.* **14**, 1–15.

Rodhe, H., Dentener, F. and Schulz, M. 2002. The global distribution of acidifying wet deposition. *Environ. Sci. Technol.* **36**, 4382–4388.

Roxy, M. K., Modi, A., Murtugudde, R., Valsala, V., Panickal, S. and co-authors. 2015a. A reduction in marine primary productivity driven by rapid warming over the tropical Indian Ocean. *Geophys. Res. Lett.* **43**, 826–833.

Roxy, M. K., Ritika, K., Terray, P., Murtugudde, R., Ashok, K. and co-authors. 2015b. Drying of Indian subcontinent by rapid Indian Ocean warming and a weakening land-sea thermal gradient. *Nat. Commun.* **6**, 7423.

Sabine, C. L., Key, R. M., Johnson, K. M., Millero, F. J., Poisson, A. and co-authors. 1999. Anthropogenic CO_2 inventory of the Indian Ocean. *Global Biogeochem. Cy.* **13**, 179–198.

Sabine, C. L., Wanninkhof, R., Key, R. M., Goyet, C. and Millero, F. J. 2000. Seasonal CO_2 fluxes in the tropical and subtropical Indian Ocean. *Mar. Chem.* **72**, 33–53.

Samanta, S., Dalai, T. K., Pattanaik, J. K., Rai, S. K. and Mazumdar, A. 2015. Dissolved inorganic carbon (DIC) and its δ13C in the Ganga (Hooghly) River estuary, India: Evidence of DIC generation via organic carbon degradation and carbonate dissolution. *Geochim. Cosmochim. Acta* **165**, 226–248.

Sarma, V., Kumar, G. S., Yadav, K., Dalabehera, H. B., Rao, D. N. and co-authors 2019. Impact of eddies on dissolved inorganic carbon components in the Bay of Bengal, *Deep Sea Res. I.* **147**, 111–120.

Sarma, V. V. S. S., Krishna, M. S., Paul, Y. S. and Murty, V. S. N. 2015. Observed changes in ocean acidity and carbon dioxide exchange in the coastal Bay of Bengal – a link to air pollution. *Tellus B: Chem. Phys. Meteorol.* **67**, 24638.

Sarma, V. V. S. S., Krishna, M. S., Rao, V. D., Viswanadham, R., Kumar, N. A. and co-authors. 2012a. Sources and sinks of CO_2 in the west coast of Bay of Bengal. *Tellus B: Chem. Phys. Meteorol.* **64**, 10961.

Sarma, V. V. S. S., Viswanadham, R., Rao, G. D., Prasad, V. R., Kumar, B. S. K. and co-authors. 2012b. Carbon dioxide emissions from Indian monsoonal estuaries. *Geophys. Res. Lett.* **39**.

Sarma, V. V. S. S., Krishna, M. S. and Srinivas, T. N. R. 2020. Sources of organic matter and tracing of nutrient pollution in the coastal Bay of Bengal. *Mar. Pollut. Bull.* **159**, 111477.

Sarma, V. V. S. S., Kumar, M. D. and George, M. D. 1998. The central and eastern Arabian Sea as a perennial source of atmospheric carbon dioxide. *Tellus B: Chem. Phys. Meteorol.* **50**, 179–184.

Sarma, V. V. S. S., Kumari, V. R., Srinivas, T. N. R., Krishna, M. S., Ganapathi, P. and co-authors. 2018. East India Coastal Current controls the dissolved inorganic carbon in the coastal Bay of Bengal. *Mar. Chem.* **205**, 37–47.

Sarma, V. V. S. S., Kumar, N. A., Prasad, V. R., Venkataramana, V., Appalanaidu, S. and co-authors. 2011. High CO_2 emissions from the tropical Godavari estuary (India) associated with monsoon river discharges. *Geophys. Res. Lett.* **38,** L08601, 1–4.

Sarma, V. V. S. S., Lenton, A., Law, R., Metzl, N., Patra, P. K. and co-authors. 2013. Sea-air CO_2 fluxes in the Indian Ocean between 1990 and 2009..

Satheesh, S. K. 2002. Letter to Editor, Aerosol radiative forcing over land: Effect of surface and cloud reflection. *Ann. Geophys.* **20**, 2105–2109.

Schlesinger, W. H. 1997. *Biogeochemistry: An Analysis of Global Change*. 2nd Edition. Academic Press, San Diego.

Sengupta, D., Bharath Raj, G. N. and Shenoi, S. S. C. 2006. Surface freshwater from Bay of Bengal runoff and Indonesian throughflow in the tropical Indian Ocean. *Geophys. Res. Lett.* **33,** L22609, 1–5.

Shankar, D., Vinayachandran, P. N. and Unnikrishnan, A. S. 2002. The monsoon currents in the north Indian Ocean. *Prog. Oceanogr.* **52**, 63–120.

Shenoi, S. S. C., Shankar, D. and Shetye, S. R. 2002. Differences in heat budgets of the near-surface Arabian Sea and Bay of Bengal: Implications for the summer monsoon. *J. Geophys. Res.* **107**, 1–5.

Shetye, S. R., Gouveia, A. D., Shankar, D., Shenoi, S. S. C., Vinayachandran, P. N. and co-authors. 1996. Hydrography and circulation in the western Bay of Bengal during the northeast monsoon. *J. Geophys. Res.* **101**, 14011–14025.

Sreenivas, P., Gnanaseelan, C. and Prasad, K. V. S. R. 2012. Influence of El Niño and Indian Ocean Dipole on sea level variability in the Bay of Bengal. *Global Planet. Change* 80–81, 215–225.

Srinivas, B., Kumar, A., Sarin, M. M. and Sudheer, A. K. 2011. Impact of continental outflow on chemistry of atmospheric aerosols over tropical Bay of Bengal. *Atmos. Chem. Phys. Discuss.* **11**, 20667–20711.

Srinivas, B. and Sarin, M. M. 2013. Atmospheric deposition of N, P and Fe to the Northern Indian Ocean: Implications to C- and N-fixation. *Sci. Total Environ.* 456–457, 104–114.

Sutton, A. J., Sabine, C. L., Dietrich, C., Maenner, J. S., Musielewicz, Sylvia, B. and co-authors. 2017. *High-resolution ocean and atmosphere pCO2 time-series measurements from mooring Mooring BOBOA_90E_15N (NCEI Accession 0162473)*. NOAA National Centers for Environmental Information. Dataset..

Suzuki, R. and Ishimatu, T. 1990. An improved method for the determination of phytoplankton chlorophyll using N, N-dimethylformamide. *J. Oceanogr.* **46**, 190–194.

Takahashi, T., Sutherland, S. C., Chipman, D. W., Goddard, J. G., Ho, C. and co-authors. 2014. Climatological distributions of pH, pCO_2, total CO_2, alkalinity, and $CaCO_3$ saturation in the global surface ocean, and temporal changes at selected locations. *Mar. Chem.* **164**, 95–125.

Takahashi, T., Sutherland, S. C., Wanninkhof, R., Sweeney, C., Feely, R. A. and co-authors. 2009. Climatological mean and decadal change in surface ocean pCO_2, and net sea-air CO_2 flux over the global oceans. *Deep-Sea Res. II.* **56**, 554–577.

Thomas, H., Prowe, A. E. F., Lima, I., Doney, S. C., Wanninkhof, R. and co-authors. 2008. Changes in the North Atlantic Oscillation influence CO_2 uptake in the North Atlantic over the past 2 decades. *Global Biogeochem. Cy.* **22**, GB4027.

Tjiputra, J. F., Olsen, A. R. E., Bopp, L., Lenton, A., Pfeil, B. and co-authors. 2014. Long-term surface pCO_2 trends from observations and models. *Tellus B: Chem. Phys. Meteorol.* **66**, 23083.

Trott, C. B., Subrahmanyam, B., Murty, V. S. N. and Shriver, J. F. 2019. Large-scale fresh and salt water exchanges in the Indian Ocean. *J. Geophys. Res. Oceans* **124**, 6252–6269.

Varkey, M. J., Murty, V. S. N. and Suryanarayana, A. 1996. Physical oceanography of the Bay of Bengal and Andaman Sea. *Oceanogr. Lit. Rev.* **5**, 413.

Vinayachandran, P. N., Murty, V. S. N. and Ramesh Babu, V. 2002. Observations of barrier layer formation in the Bay of Bengal during summer monsoon. *J. Geophys. Res.* **107**, SRF 19-1–SRF 19-9.

Weller, R., Farrar, J. T., Buckley, J., Matthew, S., Venkatesan, R. and co-authors. 2016. Air-sea interaction in the Bay of Bengal. *Oceanography* **29**, 28–37. http://dx.doi.org/10.5670/oceanog.2016.36.

Wijesekera, H. W., Shroyer, E., Tandon, A., Ravichandran, M., Sengupta, D. and co-authors. 2016. ASIRI: An ocean–atmosphere initiative for Bay of Bengal. *Bull. Am. Meteorol. Soc.* **97**, 1859–1884.

Yadav, K., Sarma, V. V. S. S. and Kumar, M. D. 2020. Spatial and temporal variability in concentration and characteristics of aerosols at Visakhapatnam (east) and Goa (west) coasts of India. *Environ. Sci. Pollut. Res. Int.* **27**, 532–536.

Yadav, K., Sarma, V. V. S. S., Rao, D. B. and Kumar, M. D. 2016. Influence of atmospheric dry deposition of inorganic nutrients on phytoplankton biomass in the coastal Bay of Bengal. *Mar. Chem.* **187**, 25–34.

Zhang, J. and Reid, J. S. 2010. A decadal regional and global trend analysis of the aerosol optical depth using a data-assimilation grade over-water MODIS and Level 2 MISR aerosol products. *Atmos. Chem. Phys.* **10**, 10949–10963.